

NASA TECHNICAL
MEMORANDUM

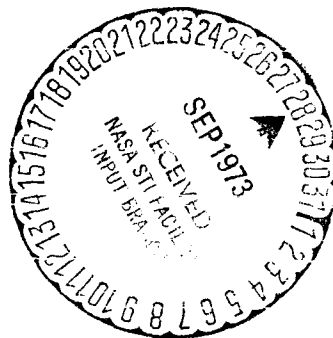
NASA TM X-2881

(NASA-TH-X-2881) COMPARISONS OF
PREDICTIONS OF THE XB-70-1 LONGITUDINAL
STABILITY AND CONTROL DERIVATIVES WITH
FLIGHT RESULTS FOR SIX FLIGHT CONDITIONS
(NASA) 44 p HC \$3.00

N73-30940

CSCL 01C

H1/02

Unclassified
12921

COMPARISON OF PREDICTIONS OF THE XB-70-1 LONGITUDINAL STABILITY AND CONTROL DERIVATIVES WITH FLIGHT RESULTS FOR SIX FLIGHT CONDITIONS

by *Chester H. Wolowicz and Roxanah B. Yancey*

*Flight Research Center
Edwards, Calif. 93523*

NATIONAL AERONAUTICS AND SPACE ADMINISTRATION • WASHINGTON, D. C. • AUGUST 1973

1. Report No. NASA TM X-2881	2. Government Accession No.	3. Recipient's Catalog No.	
4. Title and Subtitle COMPARISON OF PREDICTIONS OF THE XB-70-1 LONGITUDINAL STABILITY AND CONTROL DERIVATIVES WITH FLIGHT RESULTS FOR SIX FLIGHT CONDITIONS		5. Report Date August 1973	
7. Author(s) Chester H. Wolowicz and Roxanah B. Yancey		6. Performing Organization Code	
9. Performing Organization Name and Address NASA Flight Research Center P. O. Box 273 Edwards, California 93523		8. Performing Organization Report No. H-773	
12. Sponsoring Agency Name and Address National Aeronautics and Space Administration Washington, D. C. 20546		10. Work Unit No. 501-98-01-00	
15. Supplementary Notes		11. Contract or Grant No.	
16. Abstract		13. Type of Report and Period Covered Technical Memorandum	
17. Key Words (Suggested by Author(s)) Stability and control characteristics Predicted and flight-determined stability and control characteristics Aeroelastic effects		18. Distribution Statement Unclassified - Unlimited	
19. Security Classif. (of this report) Unclassified	20. Security Classif. (of this page) Unclassified	21. No. of Pages 42	22. Price* \$3.00

* For sale by the National Technical Information Service, Springfield, Virginia 22151

COMPARISON OF PREDICTIONS OF THE XB-70-1 LONGITUDINAL STABILITY
AND CONTROL DERIVATIVES WITH FLIGHT RESULTS
FOR SIX FLIGHT CONDITIONS

Chester H. Wolowicz and Roxanah B. Yancey
Flight Research Center

INTRODUCTION

One of the many objectives of the XB-70-1 flight-test program was an assessment of the state of the art of predicting stability and control derivatives for large flexible airplanes using the modal method of analysis (ref. 1). Knowledge of the state of the art is considered essential to the development of advanced supersonic technology.

Preliminary correlations of flight-determined and predicted stability and control characteristics for the XB-70 were made in reference 2. However, there were several areas of high uncertainty in the predictions which could have affected in particular the longitudinal characteristics. The predicted flexible airplane characteristics were based primarily on wind-tunnel data of a rigid, jig-shaped model equipped with single panel elevons, whereas the airplane had segmented elevons. Very limited data were available at that time for the segmented elevons and hence were not used. Later investigation showed that these and supplementary segmented-elevon data were compromised by the flexibility of the strain gages in the right-hand elevon segments and the free play between the gages and segments. The data were also suspect because it was believed that flexibility of unknown magnitude existed in the model due to its frequent reworking over a period of years. In addition, the predicted effects of flexibility were based on projected mass distributions that were not necessarily representative of the flight-test conditions of the full-scale airplane.

An opportunity arose to obtain new predictions of longitudinal characteristics for selected actual flight-test conditions as part of a follow-on NASA study to assess the predictability of airplane cruise drag at a Mach number of 2.53. For this study, a model was built as near as possible to the deformed shape of the airplane in the cruise condition. It was felt that the relatively small deformations in the model for this flight condition would result primarily in incremental shifts in the normal force and pitching-moment characteristics, but that the slopes of the curves would not change significantly. Thus, it was expected that the stability derivatives would not be affected by the deformations.

The North American Rockwell Corporation, designer of the XB-70, was contracted to define the shape of the model and to design and build the model for testing in the Ames 11- by 11-foot and 9- by 7-foot tunnels. The contract included updating the original predictions for the longitudinal characteristics (ref. 3) for the rigid jig-shaped and flexible aircraft for six actual flight-test conditions considering all previous as well as the new model data.

This report presents results of the contractor's revision of its original estimates and compares the earlier (ref. 3) and updated predictions (ref. 4) with flight-determined results. The flight-determined characteristics were obtained by three different techniques to establish the most probable flight values.

SYMBOLS

Physical quantities in this report are given in the International System of Units (SI) and parenthetically in U.S. Customary Units. The measurements were taken in U.S. Customary Units. Factors relating the two systems are presented in reference 5.

The data are presented in the form of standard NASA coefficients of forces and moments, which are referred to the body axes passing through the center of gravity. The positive directions are: X, forward; Y, to the right; and Z, down. Positive directions of the forces, moments, angular displacements, and velocities are in accord with the right-hand rule. All derivatives are in radians unless otherwise noted.

a_n normal acceleration, g

C_L lift coefficient

C_m pitching-moment coefficient

$$C_m = \frac{\partial C_m}{\partial \frac{q \bar{c}_w}{2V}}$$

$$(\bar{C}_m)_q = - \frac{c_1^2}{\bar{c}_w} (\bar{C}_m)_{\alpha_c} \Big|_R$$

C_{m_α} static stability parameter, $\frac{\partial C_m}{\partial \alpha}$

$$C_{m_{\alpha_c}} = \frac{\partial C_m}{\partial \alpha_c}$$

$$(\bar{C}_m)_{\alpha_c} = (C_{m_{\alpha_c}})_{\alpha_c} + (C_{m_{\alpha_c}})_{I_R}$$

$$C_{m_{\dot{\alpha}}} = \frac{\partial C_m}{\partial \frac{\dot{\alpha} \bar{c}_w}{2V}}$$

$$C_{m_{\delta_c}} = \frac{\partial C_m}{\partial \delta_c}$$

$$\left(\bar{C}_{m_{\delta_c}} \right) = \left(C_{m_{\delta_c}} \right)_R + \left(C_{m_{\delta_c}} \right)_{I_R}$$

$$C_{m_{\delta_e}} = \frac{\partial C_m}{\partial \delta_e}$$

$$C_{m_{\bar{\delta}_e}} = C_{m_{\delta_e}} + \frac{\delta_c}{\delta_e} \left(C_{m_{\delta_c}} \right)$$

$$C_N \quad \quad \quad \text{normal-force coefficient}$$

$$C_{N_q} = \frac{\partial C_N}{\partial \frac{q \bar{c}_w}{2V}}$$

$$\left(\bar{C}_{N_q} \right)_{c_R} = - \frac{2 \frac{1}{c_1}}{\bar{c}_w} \left(\bar{C}_{N_{\alpha_c}} \right)_R$$

$$C_{N_{\alpha}} \quad \quad \quad \text{normal-force curve slope,} \quad \frac{\partial C_N}{\partial \alpha}$$

$$C_{N_{\alpha_c}} = \frac{\partial C_N}{\partial \alpha_c}$$

$$\left(\bar{C}_{N_{\alpha_c}} \right)_R = \left(C_{N_{\alpha_c}} \right)_R + \left(C_{N_{\alpha_c}} \right)_{I_R}$$

$$C_{N_{\dot{\alpha}}} = \frac{\partial C_N}{\partial \frac{\dot{\alpha} \bar{c}_w}{2V}}$$

$$C_{N_{\delta_c}} = \frac{\partial C_N}{\partial \delta_c}$$

$$\left(\bar{C}_{N_{\delta_c}}\right)_R = \left(C_{N_{\delta_c}}\right)_R + \left(C_{N_{\delta_c}}\right)_{I_R}$$

$$C_{N_{\delta_e}} = \frac{\partial C_N}{\partial \delta_e}$$

$$C_{N_{\bar{\delta}_e}} = C_{N_{\delta_e}} + \frac{\delta_c}{\delta_e} \left(C_{N_{\delta_c}}\right)$$

$$\bar{c}_w$$

wing mean aerodynamic chord, m (in.)

$$\left(\frac{F}{R}\right)_{C_{m_\alpha}}, \left(\frac{F}{R}\right)_{C_{N_\alpha}}$$

flexible-to-rigid ratio of C_{m_α} and C_{N_α}

$$\left(\frac{F}{R}\right)_{\bar{C}_{m_\alpha}}, \left(\frac{F}{R}\right)_{\bar{C}_{N_\alpha}}$$

flexible-to-rigid ratio of C_{m_α} and C_{N_α} including interference

$$\left(\frac{F}{R}\right)_{\bar{C}_{m_{\delta_c}}}, \left(\frac{F}{R}\right)_{\bar{C}_{N_{\delta_c}}}$$

flexible-to-rigid ratio of $C_{m_{\delta_c}}$ and $C_{N_{\delta_c}}$ including interference

$$g$$

acceleration due to gravity, m/sec^2 (ft/sec^2)

$$h_p$$

pressure altitude, m (ft)

$$I_Y$$

moment of inertia about the Y-axis, $kg \cdot m^2$ ($slug \cdot ft^2$)

$$l_{c_1}$$

longitudinal distance between the canard center of pressure and the center of gravity, m (ft)

l_{c_2}	longitudinal distance between the three-quarter chord point on the canard mean aerodynamic chord and the three-quarter chord point on the wing mean aerodynamic chord, m (ft)
M	Mach number
N_{Re}	Reynolds number
P	period of the transient oscillations, sec
q	pitching rate, rad/sec or deg/sec
\dot{q}	pitching acceleration, rad/sec ²
\bar{q}	dynamic pressure, N/m ² (lb/ft ²)
S_w	wing area, m ² (ft ²)
$T_{1/2}$	time required for the transient oscillation to damp to half amplitude, sec
t	time, sec
V	airspeed, m/sec (ft/sec)
v	vertical stabilizer
W	airplane weight, kg (lb)
wf	wing/fuselage
α	angle of attack, deg or rad
α_c	angle of attack of canard, deg or rad
$\dot{\alpha}$	rate of change with time of angle of attack, rad/sec
Δ	increment
δ_c	canard deflection, deg
δ_e	elevator deflection, deg
δ_T	wingtip deflection, deg
ξ	damping ratio

θ	pitch angle, deg
ω_n	undamped natural frequency of the transient oscillation, rad/sec
ω_{n_d}	damped natural frequency of the transient oscillation, rad/sec

Subscripts:

c	canard
F	flexible airplane
I	canard interference (acting on the wing)
R	jig-shaped rigid airplane (undeformed)

The symbol $||$ represents the absolute magnitude of a quantity. The phase angle of a vector j relative to another vector k is indicated by Φ_{jk} , with the second subscript used as the reference.

THE AIRPLANE

The XB-70-1 airplane (fig. 1) has a design gross weight in excess of 226,800 kilograms (500,000 pounds) and a design cruising speed of Mach 3.0 at approximately 21,300 meters (70,000 feet) altitude. It has a thin, low-aspect-ratio, highly swept delta wing with folding wingtips, twin movable vertical stabilizers, elevon surfaces for pitch and roll control, a movable canard with trailing-edge flaps, and twin inlets enclosed in a single nacelle. The physical characteristics of the airplane are given in table 1.

The normal operational limits for the three wingtip configurations are shown in figure 2.

The elevons are split into six spanwise segments on each wing semispan to prevent binding due to wing bending. When the wingtips are in the deflected position, the two outboard segments on each tip are faired at a zero setting and become part of the folded tip.

The canard surface provides part of the pitch control and has a flap for use during takeoff and landing. For normal takeoffs and landings, the forepart of the canard is fixed at an incidence of 0° and the canard flap is full down at 20° . In the normal flight configuration, the canard is geared to the elevons in the ratio of $\frac{\delta_c}{\delta_e} = -0.15$, as shown in figure 3. As noted in reference 4, flight data showed the gearing curve to have the same slope as the design gearing but with an offset

depending on the flight condition. At Mach numbers of 0.75, 1.22, 1.61, and 2.39 with the pitch augmentation off, the curves were offset by approximately -0.5° , -1.5° , -1.4° , and 1.5° of elevator deflection, respectively.

FLIGHT-TEST CONDITIONS INVESTIGATED

The six flight-test conditions selected for updating the predicted longitudinal stability and control derivatives are summarized in table 2. The coding of the case numbers corresponds to the coding used in reference 4. The Mach numbers and pressure altitudes shown are corrected indicated flight values, with the corrections applied in accordance with procedures used at the NASA Flight Research Center. The weights and centers of gravity are updated values provided by North American Rockwell Corporation during the present investigation.

UPDATING THE PREDICTED CHARACTERISTICS

Updating the predicted characteristics for the six flight-test conditions involved a review of weight and inertia data, structural mode characteristics, aerodynamic data for the rigid airplane, and the rigid and flexible airplane stability and control characteristics as outlined in the following sections.

Weight and Inertia

The predicted stability and control derivatives summarized in reference 3 were based on early estimates of weight, weight distributions, and consequent flexibility effects for various flight conditions. A review of the airplane's weight and weight distribution history through the flight-test program showed considerable deviations in empty weight due to equipment and ballast changes and structural repair.

The first step in updating the predicted characteristics involved correcting the empty airplane weight distribution and pitch moments of inertia as well as establishing a grid pattern for the corrected weight distribution for each of the six flight conditions being investigated. The known empty weight distribution of flight 50, which was essentially identical to that used in ground vibration tests, was used as a starting point. The weight change logs for subsequent flights were reviewed to update the empty weight distribution for the six flight conditions being investigated. The weight and the weight distribution of the fuel and the other consumables for each flight were obtained from flight records.

With the weight distribution of the empty airplane and consumables accounted for, the updated total airplane weight, weight grid, center of gravity, and pitch inertia were determined for each flight case.

Structural Mode Characteristics

The updated distributed and total weights and inertias were used to obtain the symmetric structural mode characteristics for each case investigated. Details of the programming procedures employed are included in reference 4.

Table 3 summarizes the calculated symmetrical free-free vibration mode characteristics for case SC-1 to illustrate a typical relationship between mode number and mode description. It should be noted that the aeroelastic analysis of reference 4 takes into account mode numbers 1, 2, 3, and 5, which correspond to the first four wing/fuselage modes. Mode number 4 is the first vertical tail mode, which is negligible in determining the longitudinal characteristics.

Rigid Airplane Aerodynamic Data

The rigid airplane aerodynamic data used in the original prediction of the stability and control characteristics (ref. 3) were the result of the filtering of static tunnel data from several tunnels, involving several jig-shaped models of various degrees of modification. With limited exceptions, the models were equipped with slab elevons and the data compiled did not account for segmentation effects.

The updating of the original data was accomplished in two phases. In phase 1, the contractor updated his original estimates to reflect the results of a more recent series of tests conducted in the NASA Ames 11- by 11-foot tunnel in December of 1966 and 1967. In these tests a more representative jig-shaped model equipped with segmented elevons containing strain gages in the right-hand segments was used. The revision of the force data included elevator effectiveness and zero-lift angle of attack. Revisions were also made in the load distributions corresponding to the flight conditions shown in table 2 to update the aeroelastic deformation effects. The calculated dynamic stability derivatives due to $\dot{\alpha}$ and \dot{q} were also revised.

Phase 2 updating of the data was undertaken when NASA Ames wind-tunnel data for the deformed model became available. The model was tested with both slab and segmented elevons without strain gage provisions. The primary difference between data obtained in 1966 and 1967 for the jig-shaped model and the data for the deformed model was the translation of the lift and pitching-moment curves, as typified in figure 4. This change was due to the differences in shape between the two models. The results for the deformed model showed a loss in control effectiveness due to segmentation that was similar although slightly less than indicated by the jig-shaped model data, as illustrated in figure 5 for an angle of attack of 0° . The discrepancy is attributed to excessive flexibility in the elevon hinge-moment strain gage installation used on the jig-shaped model. The phase 1 revisions of elevator effectiveness curves for $C_{N_{\delta_e}}$ and $C_{m_{\delta_e}}$ were modified to reflect the results for the segmented elevons on the deformed model, which did not contain the strain gages.

The effects of the bypass doors on trim and stability characteristics, although small for the flight-test conditions investigated, were included in the updated force data. The effects of the bypass doors were not included in the original estimates.

The change in trim due to the presence of the inlet boundary-layer bleed sugar scoop, which was located below and slightly aft of the inlets, was investigated on the deformed model with no airflow through the sugar scoop duct. Although the scoop had no effect on the slope of the pitching-moment curve, it did add a small destabilizing pitching moment which warranted inclusion in the updated predictions. Effects of boundary-layer bleed through the flow diverter located at the top of the inlet were not included because of the lack of experimental data in the Mach number range pertinent to the flight conditions of this report.

The dynamic derivatives C_{m_q} and C_{N_q} , which are included in reference 3, were calculated on the basis of theory and correlations with existing experimental data from configurations with similar components. This approach was reevaluated and new data were generated as explained in reference 4.

The dynamic derivatives $C_{m_{\dot{\alpha}}}$ and $C_{N_{\dot{\alpha}}}$, which were omitted from reference 3, were included in the updating as explained in reference 4. The wing was the primary component considered. Although the influence of $\dot{\alpha}$ on the canard was considered negligible, the effect of downwash lag from the canard on the wing was included. The effect of the fuselage on the $\dot{\alpha}$ derivatives was assumed to be negligible.

Generalized Aerodynamic Data for Mode Forces

Generalized aerodynamic data for structural mode forces were reevaluated using lifting surface theory programs that had not been used in the original predictions. According to reference 4, the use of these programs resulted in improved data.

Generalized fuselage forces were also upgraded. In the original analysis, a point load at the center of pressure for the rigid airplane was assumed. In the review, a modified slender-body theory was used to obtain a distributed load for the purpose of obtaining the generalized modal forces.

Predicted Rigid and Flexible Airplane Stability and Control Characteristics

Using updated structural mode characteristics, aerodynamic data for the rigid (undeformed) airplane, and generalized aerodynamic data for mode forces, the predicted stability and control derivatives for the airplane at 1g conditions were determined by the contractor using a 17-degree-of-freedom computer program. The program has a wide range of capabilities in five rigid body degrees of freedom including component buildup, moment reference transfer, flexible-to-rigid ratios, and so forth. The appropriate program elements were used along with the first four symmetric wing/fuselage structural modes (the same number employed in the original predictions) to obtain the derivatives for the six flight conditions listed in table 2. The analysis was accomplished for both the rigid (undeformed) and the flexible airplane conditions.

The recognition of nonlinearities in the aerodynamic data is essential for the accurate prediction of steady-state trim characteristics and the subsequent

determination of the derivatives about the trim points. Nonlinear aerodynamic data were entered into the program in the form of coefficients wherever the data permitted. The equations of motion for rigid body and symmetric structural modes were also in coefficient form to be compatible with the nonlinear aerodynamics.

After establishing the trim conditions, the aerodynamic data were linearized by taking the local slopes of the curves at the trim point. The linearized model was then used to compute the flexible-to-rigid ratios of the various aerodynamic parameters. The technique for obtaining flexible-to-rigid ratios from modal data is discussed in appendix D of reference 4.

The updated longitudinal stability and control derivatives for the rigid airplane at the flight-test conditions of table 2 are summarized in table 4. These derivatives, from reference 4, include listings of contributions from the wing/body, elevator, canard, and canard-interference components. The updated flexible-to-rigid ratios for the various components as well as the complete airplane are listed in table 5. The information contained in tables 4 and 5 was combined to obtain the updated predictions of rigid and flexible airplane derivatives for each of the six flight-test conditions of table 2. The results are summarized in tables 6 through 9.

ACQUISITION OF THE FLIGHT DATA

The flight-determined derivatives were obtained from an analysis of time histories of elevator-pulse maneuvers typified by figure 6. The data were obtained from a pulse-code-modulated (PCM) system wherein the sensor signals were converted to digital format and stored on magnetic tape on a time-sharing basis with other data. Details of the instrumentation pertinent to the stability and control investigation are presented in reference 2.

The sensor signals were sampled at the rate of 20 samples per second, which, as shown in figure 6, was sufficient to provide good definition of the entire time history of the normal acceleration and pitch-rate responses. However, as also shown by the figure, the latter portions of the elevator position, pitch acceleration, pitch attitude, and angle of attack time histories were poorly defined. This deficiency was overcome by careful fairing of the data points with due consideration for the period and damping characteristics obtained from the normal acceleration and pitch-rate time histories. The final fairings showed that an oscillatory elevator movement was induced by the pitch rate during the entire transient portion of the maneuver.

The time histories of pitch rate and pitch acceleration indicated a lag of approximately 0.2 second, which necessitated a shift of these data by the same amount to obtain proper phase relationship with the other responses.

ANALYSIS OF THE FLIGHT DATA

Three methods of analysis were employed to establish the most probable flight values of the derivatives; namely, the graphical time-vector technique (ref. 6), the analog-matching technique (ref. 2), and the modified Newton-Raphson technique

(refs. 7 and 8). Each method was applied by a different analyst who faired the flight data on the basis of his own judgment.

Time-Vector Technique

The time-vector technique was applied in accordance with the procedures outlined in reference 6, but with one modification. Normally, the technique is applied to the transient portion of an oscillatory maneuver with the controls fixed. In the present instance, the elevator moved in an oscillatory manner, and this movement had to be taken into account. Table 10 summarizes the pertinent flight-determined short-period characteristics essential to the time-vector analysis. The table shows

that the amplitude ratio $\left| \frac{\delta_e}{\alpha} \right|$ was generally larger than 0.4 and that the phase angle $\Phi_{\delta_e \alpha}$ was generally between -70° and -80° . The elevator motion vector was generally between -150° and -160° out of phase with respect to the pitch-rate vector.

The derivative C_{N_α} was determined by the relationship

$$C_{N_\alpha} = \frac{W}{\bar{q}S_w} \left| \frac{a_n}{\alpha} \right|$$

Elevator motion had no significant effect on this derivative. It was not possible, however, to obtain $C_{N_q} + C_{N_{\dot{\alpha}}}$ or $C_{N_{\delta_e}}$ with any reasonable degree of accuracy, since

these quantities are approximately normal to the vector for C_{N_α} in a vector diagram

and are critically dependent upon a precise determination of the relatively small phase angle $\Phi_{a_n \alpha}$ (table 10). This angle could not be measured to the requisite precision.

The pitching-moment derivatives, including $C_{m_{\delta_e}}$, were amenable to solution using an iterative procedure. A first approximation of the derivatives C_{m_α} and $C_{m_q} + C_{m_{\dot{\alpha}}}$ was obtained from a vector diagram like the one illustrated in figure 7(a) with the elevator motion neglected. (Fig. 7(b) shows a final solution.) These initial values from figure 7(a) were then used in the transposed pitching-moment equation shown in figure 8 in conjunction with the initial input and corresponding responses to obtain a first approximation of $C_{m_{\delta_e}}$ as shown. This value of $C_{m_{\delta_e}}$ was then used to obtain a vector diagram similar to figure 7(b) to complete the first iteration of C_{m_α} and $C_{m_q} + C_{m_{\dot{\alpha}}}$. The process was repeated through successive iterations to convergence. Figure 7(b) and figure 8 show the converged solutions for C_{m_α} ,

$C_{m_q} + C_{m_{\dot{\alpha}}}$, and $C_{m_{\bar{\delta}_e}}$ for case SC-2.

Analog-Matching Technique

The analog-matching procedures described in reference 2 were used to analyze four of the six cases listed in table 10. The minor derivative $C_{N_q} + C_{N_{\dot{\alpha}}}$ was particularly difficult to identify since it is a weak derivative and its determination is sensitive to slight phase errors in angle of attack and pitch rate. The analyst generally estimated the most likely value based on his experience with the time histories analyzed.

Modified Newton-Raphson Technique

The modified Newton-Raphson method used in the analysis is an automated output-error technique developed at the NASA Flight Research Center. This method substantially reduces computation time and minimizes dependence on the skill of an analyst. The method incorporates an a priori feature which allows data with deficiencies or abnormalities to be successfully analyzed. With the a priori provision included, the flight-determined derivatives may be biased in favor of the best a priori estimates available (manufacturer's data, in the present instance). If sufficient information is available in the flight responses to define the derivative, the a priori estimate has little influence on the derivative obtained from the analysis. On the other hand, a derivative poorly defined because of insufficient information in the responses tends to equal the a priori estimate. Consequently, if there is close agreement in the values of a derivative obtained without and with a priori estimates, the derivative is well defined. If the values are far apart, there is insufficient information in the flight responses to define the derivative. Detailed information regarding the method may be obtained from references 7 and 8.

COMPARISON OF PREDICTED AND FLIGHT-DETERMINED CHARACTERISTICS

The original and updated predicted characteristics, both rigid and elastic, as well as the flight-determined characteristics, are summarized in table 11 and in figures 9(a) and 9(b) for the six flight conditions investigated. The results are discussed in the following sections.

Normal-Force Derivatives

In figure 9(a), the changes in $C_{N_{\alpha}}$ due to the updating are insignificant.

Aeroelastic effects decrease the magnitude of the derivative in each of the six cases. The heavyweight and lightweight subsonic flight data at $M = 0.76$ and $M = 0.75$ (SC-1 and SC-2) indicate significantly higher values of $C_{N_{\alpha}}$ than predicted from tests of either rigid or flexible models. A similar difference can be observed in the

lightweight transonic case (SC-4, $M = 1.22$) and to a lesser extent in the supersonic case (SC-6, $M = 1.61$). For the remaining two cases (SC-3, $M = 1.22$ and SC-7, $M = 2.39$) the correlation of the predictions and the flight data is good.

The updated rigid model values for the derivative $C_{N_{\bar{\delta}}}$ show a significant difference from the original estimates (based on nonsegmented elevons) which is due primarily to the segmentation of the elevons. It should be noted that the updated predicted values of this derivative for the elastic airplane show greatly reduced aeroelastic corrections. The flight data for $C_{N_{\bar{\delta}}}$ generally are much lower than the

updated predictions and imply a deficiency in the correction for aeroelastic effects. It is interesting to note that if the aeroelastic correction for the updated predictions had been the same as for the original predictions, the predicted values would have tended toward agreement with the flight data.

The combined dynamic derivative $C_{N_q} + C_{N_{\dot{\alpha}}}$ is normally neglected; it has a negligible effect on dynamic response, and, in addition, it is difficult to predict and to extract from flight data. It is included here to illustrate its sensitivity to the method of analysis. Figure 9(a) shows that the updating of the theoretical rigid values of the dynamic derivative resulted in large changes for the subsonic cases, but negligible changes for the transonic and supersonic cases. Also, the corrections for aeroelastic effects in the updated values appear to be negligible. Figure 10 shows that the large changes in the updated predicted subsonic cases are due mainly to the change in C_{N_q} , the inclusion of $C_{N_{\dot{\alpha}}}$ (originally neglected), and a reduction in the aeroelastic effects. In the transonic and supersonic cases (fig. 10), the predicted aeroelastic effects for C_{N_q} and $C_{N_{\dot{\alpha}}}$ tend to cancel.

Prior to establishing the original predictions for C_{N_q} and $C_{N_{\dot{\alpha}}}$, the manufacturer obtained preliminary estimates of these derivatives for rigid airplane conditions on the basis of numerous theoretical and experimental NASA research memorandums. These preliminary estimates, summarized in reference 4, are shown in figure 11. A comparison of figures 10 and 11 shows that the preliminary estimates of rigid airplane C_{N_q} in figure 11 are smaller than those in figure 10. Also, the sign of the preliminary estimates of the rigid airplane $C_{N_{\dot{\alpha}}}$ is opposite to the sign of the values listed in figure 10. It should be noted that the preliminary estimates used basic supersonic theories with results extrapolated to subsonic speed, whereas the updated estimates used state-of-the-art double lattice theory (for subsonic conditions) and Mach box theory (for supersonic conditions).

Pitching-Moment Derivatives

Figure 9(b) shows the original and updated predicted rigid model values of C_{m_α} to be similar. The aeroelastic corrections are less for the updated than for the original predictions. The large decrease in the aeroelastic correction in case SC-1 is believed to be incorrect considering the trend of the comparisons in all the other cases. The flight data are generally consistent and appear to correlate better with the updated predictions than with the original predictions (except in case SC-1).

The updated rigid model values of $C_{m_{\delta_e}}$, like $C_{N_{\delta_e}}$, show a significant difference from the original estimates (based on nonsegmented elevons) due primarily to the segmentation of the elevons. Here too the updating resulted in greatly reduced aeroelastic corrections, tending to bring the original and updated aeroelastic values (except for case SC-2) into closer agreement. The flight data generally agree well with both the original and the updated predictions.

The updated predicted subsonic rigid values of $C_{m_q} + C_{m_{\dot{\alpha}}}$ shown in figure 9(b) indicate a relatively large increase in the derivative compared with the original predictions. This increase is due both to changes in C_{m_q} and the addition of $C_{m_{\dot{\alpha}}}$, which was neglected in the original estimates (see fig. 10). The updated elastic corrections are negligible, as shown in figure 10. The updated transonic and supersonic rigid values of $C_{m_q} + C_{m_{\dot{\alpha}}}$ shown in figure 9 indicate negligible changes compared with the original values as a result of the compensating changes between $C_{m_{\dot{\alpha}}}$ and C_{m_q} . The small size of the corrections for aeroelasticity in the updated derivatives is also due to the tendency for $C_{m_{\dot{\alpha}}}$ and C_{m_q} to cancel one another. Although the updated estimates of $C_{m_q} + C_{m_{\dot{\alpha}}}$ were expected to show better correlation with the flight data than the original estimates, the flight data appear to be in better agreement with the original estimates.

CONCLUDING REMARKS

A reevaluation and updating of the predicted longitudinal stability and control characteristics of the XB-70-1 airplane for six specific flight-test conditions resulted in improved correlation with flight-determined values of the variation of pitching-moment coefficient with angle of attack.

In four of the six cases involving the variation of the normal-force coefficient with angle of attack, the flight values were higher than predicted; flight results and predictions showed good correlation in the remaining two cases.

The trend of the flight data indicated that the predicted subsonic and transonic values of the variation of the normal-force coefficient with elevator-canard deflection should be lower.

The flight-determined pitch-damping derivative $C_{m_q} + C_{m\dot{\alpha}}$ showed better correlation with the original theoretical estimates than with the updated predictions.

It appears, in general, that additional studies are required in the application of aeroelastic corrections to rigid model wind-tunnel data and the theoretical determination of dynamic derivatives for this class of aircraft.

Flight Research Center,
National Aeronautics and Space Administration,
Edwards, Calif., April 12, 1973.

REFERENCES

1. Wykes, John H.; and Lawrence, Robert E.: Aerothermoelasticity—Some Recent Studies of the Impact on Stability and Control of Winged Aerospace Vehicles. AIAA Paper No. 64-489, July 1964.
2. Wolowicz, Chester H.; Strutz, Larry W.; Gilyard, Glenn B.; and Matheny, Neil W.: Preliminary Flight Evaluation of the Stability and Control Derivatives and Dynamic Characteristics of the Unaugmented XB-70-1 Airplane Including Comparisons With Predictions. NASA TN D-4578, 1968.
3. Aerodynamics Group: Estimated Rigid and Flexible Aerodynamic Derivatives for XB-70 Air Vehicle No. 1. Rep. No. TFD-65-396, North American Aviation, Inc., June 21, 1965.
4. Wykes, John H.; and Lawrence, Robert E.: Estimated Performance and Stability and Control Data for Correlation With XB-70-1 Flight Test Data. NASA CR-114335, 1971.
5. Mechtly, E. A.: The International System of Units - Physical Constants and Conversion Factors. NASA SP-7012, 1969.
6. Wolowicz, Chester H.: Considerations in the Determination of Stability and Control Derivatives and Dynamic Characteristics From Flight Data. AGARD Rep. 549-Part 1, 1966.
7. Iliff, Kenneth W.; and Taylor, Lawrence W., Jr.: Determination of Stability Derivatives From Flight Data Using a Newton-Raphson Minimization Technique. NASA TN D-6579, 1972.
8. Wolowicz, Chester H.; Iliff, Kenneth W.; and Gilyard, Glenn B.: Flight Test Experience in Aircraft Parameter Identification. Paper 23, AGARD CP-119, 1972.

TABLE 1. — GEOMETRIC CHARACTERISTICS OF THE XB-70-1 AIRPLANE

Wing —		
Total area, includes 230.62 m^2 (2482.34 ft^2) covered by fuselage but not 3.12 m^2 (33.53 ft^2) of the wing ramp area, m^2 (ft^2)	585.07 (6297.8)	
Span, m (ft)	32 (105)	
Aspect ratio	1.751	
Taper ratio019	
Dihedral angle, deg	0	
Root chord (wing station 0), m (ft)	35.89 (117.76)	
Tip chord (wing station 16 m (630 in.)), m (ft)67 (2.19)	
Mean aerodynamic chord, m (in.)	23.94 (942.38)	
Wing station, m (in.)	5.43 (213.85)	
Fuselage station of 25-percent wing mean aerodynamic chord, m (in.)	41.18 (1621.22)	
Sweepback angle, deg:		
Leading edge	65.57	
25-percent element	58.79	
Trailing edge	0	
Airfoil section30 to .70 HEX (MOD)	
Thickness, percent chord:		
Wing station —		
Root to 4.72 m (186 in.)	2.0	
11.68 m to 16 m (460 in. to 630 in.)	2.5	
Folding wingtip (data for one tip only) —		
Area, m^2 (ft^2)	48.39 (520.90)	
Span, m (ft)	6.33 (20.78)	
Aspect ratio829	
Taper ratio046	
Root chord (wing station 9.67 m (380.62 in.)), m (ft)	14.61 (47.94)	
Tip chord (wing station 16 m (630 in.)), m (ft)67 (2.19)	
Mean aerodynamic chord (wing station 11.87 m (467.37 in.)), m (in.)	9.76 (384.25)	
Down deflection from inboard wing, deg	0, 25, 65	
Elevons (data for one side) —		
Total effective area aft of hinge line, includes 0.31 m^2 (3.33 ft^2) air gap at wingtip fold line, m^2 (ft^2)	18.37 (197.7)	
Span, m (ft):		
Wingtips up	6.23 (20.44)	
Wingtips down	4.26 (13.98)	
Chord, m (in.)	2.95 (116)	
Sweepback of hinge line, deg	0	

TABLE 1. — GEOMETRIC CHARACTERISTICS OF THE XB-70-1 AIRPLANE - Concluded

Canard —

Area, includes 13.96 m ² (150.31 ft ²) covered by fuselage,	
m ² (ft ²)	38.61 (415.59)
Span, m (ft)	8.78 (28.81)
Aspect ratio	1.997
Taper ratio388
Dihedral angle, deg	0
Root chord (canard station 0), m (ft)	6.34 (20.79)
Tip chord (canard station 4.39 m (172.86 in.)), m (ft)	2.46 (8.06)
Mean aerodynamic chord, m (in.)	4.68 (184.3)
Canard station, m (in.)	1.87 (73.71)
Fuselage station of 25-percent chord, m (in.)	14.06 (553.73)
Sweepback angle, deg:	
Leading edge	31.70
25-percent element	21.64
Trailing edge	-14.91
Airfoil section34 to .66 HEX (MOD)
Thickness chord ratio, percent:	
Root	2.5
Tip	2.52
Ratio of canard area to wing area066
Canard flap (data for one side) —	
Area (aft of hinge line), m ² (ft ²)	5.08 (54.69)
Inboard chord (canard station 1.22 m (47.93 in.)), m (ft) . .	2.18 (7.16)
Outboard chord (canard station 4.39 m (172.86 in.)), m (ft) .	1.02 (3.34)
Ratio of flap area to canard semiarea263
Fuselage (includes canopy) —	
Length, m (ft)	56.62 (185.75)
Maximum depth (fuselage station 22.30 m (878 in.)), m (in.)	2.72 (106.92)
Maximum breadth (fuselage station 21.72 m (855 in.)), m (in.)	2.54 (100)
Side area, m ² (ft ²)	87.30 (939.72)
Planform area, m ² (ft ²)	110.07 (1184.78)

TABLE 2. — XB-70-1 STABILITY AND CONTROL FLIGHT-TEST CONDITIONS INVESTIGATED

	Case number					
	SC-1	SC-2	SC-3	SC-4	SC-6	SC-7
Flight number	63	63	64	75	81	68
Data time	0: 36: 49	1: 55: 57	0: 35: 30	2: 04: 0.5	1: 50: 26	1: 53: 23
M	0.76	0.75	1.22	1.22	1.61	2.39
h_p , m (ft)	4720 (15,500)	7650 (25,100)	9880 (32,400)	11,980 (39,300)	11,770 (38,600)	17,100 (56,100)
W, kg (lb)	2.179×10^5 (4.804×10^5)	1.541×10^5 (3.396×10^5)	1.921×10^5 (4.235×10^5)	1.622×10^5 (3.575×10^5)	1.871×10^5 (4.125×10^5)	1.747×10^5 (3.852×10^5)
Center of gravity, percent c_w	22.1	23.4	22.8	20.9	22.0	21.2
I_Y , $\text{kg}\cdot\text{m}^2$ (slug-ft 2)	2.957×10^7 (2.181×10^7)	2.418×10^7 (1.783×10^7)	2.848×10^7 (2.100×10^7)	2.594×10^7 (1.913×10^7)	2.869×10^7 (2.116×10^7)	2.798×10^7 (2.063×10^7)
δ_T , deg	0	0	25	25	65	65
α , deg	4.5	4.4	3.7	4.7	3.2	3.7
δ_e , deg	3.8	2.6	10.9	6.7	10.2	4.6
δ_c , deg	2.36	2.58	1.18	1.73	1.26	2.54
a_n , g	1.0	1.0	1.0	1.0	1.0	1.0
Bypass door position, deg	Closed	Closed	1.00	1.00	3.50	5.00
Nose ramp position	Down	Down	Down	Down	Down	Down
V, m/sec (ft/sec)	244 (802)	232 (762)	362 (1191)	359 (1181)	474 (1559)	703 (2314)
\bar{q} , N/m 2 (lb/ft 2)	22,645 (475)	14,745 (310)	27,675 (580)	20,300 (425)	36,535 (765)	34,855 (730)
C_L	0.1614	0.1748	0.1163	0.1325	0.0857	0.0841

TABLE 3. — SYMMETRIC FREE-FREE VIBRATION MODE
CHARACTERISTICS FOR CASE SC-1

[From ref. 4]

Mode number	Mode description ¹	Frequency, hertz
1	wf 1	2.2940
2	wf 2	3.6118
3	wf 3	5.0595
4	v 1	6.0072
5	wf 4	6.7391
6	wf 5	8.0921
7	c 1	9.3665
8	wf 6	10.0762
9	wf 7	14.8513
10	wf 8	19.7754
11	v 2	22.3180
12	wf 9	24.7003
13	v 3	26.4425
14	c 2	26.7170
15	c 3	40.3209
16	c 4	52.0604

¹wf refers to wing/fuselage.

v refers to vertical stabilizer.

c refers to canard.

TABLE 4. — PREDICTED RIGID AIRPLANE STABILITY AND CONTROL DERIVATIVES
FOR FLIGHT-TEST CONDITIONS INVESTIGATED

[From ref. 4; all derivatives are in radians]

	Case number					
	SC-1	SC-2	SC-3	SC-4	SC-6	SC-7
$(C_{N\alpha})_{wf_R}$	2.5302	2.5273	2.3862	2.4310	1.7696	1.3995
$(C_{N\alpha_c})_R$.23457	.23354	.23435	.24616	.19468	.12613
$(C_{N\alpha_c})_{I_R}$	-.22744	-.22643	-.22114	-.22754	-.13404	-.03675
$(C_{N\delta_c})_R$.17537	.17588	.17095	.17309	.14194	.09488
$(C_{N\delta_c})_{I_R}$	-.15466	-.15401	-.15388	-.15272	-.10116	-.02609
$(C_{N\delta_e})_R$.43960	.44044	.09911	.09727	.07371	.04392
$(C_{N\dot{\alpha}})_{wf_R}$	1.1100	1.1200	.00420	.00420	-.07600	---
$(C_{Nq})_{wf_R}$	3.3475	3.1859	2.3049	2.3690	1.1310	.53590
$(C_{m\alpha})_{wf_R}$	-0.42680	-0.39157	-0.55483	-0.60661	-0.34879	-0.26654
$(C_{m\alpha_c})_R$.24321	.24596	.25284	.24950	.21258	.13605
$(C_{m\alpha_c})_{I_R}$	-.04594	-.04890	-.05808	-.05219	-.05631	-.02654
$(C_{m\delta_c})_R$.19078	.19380	.18337	.18194	.15080	.09834
$(C_{m\delta_c})_{I_R}$	-.03526	-.03767	-.04390	-.04158	-.03588	-.00652
$(C_{m\delta_e})_R$	-.22406	-.21788	-.06819	-.06897	-.05200	-.03243
$(C_{m\dot{\alpha}})_{wf_R}$	-.46800	-.44700	.23600	.23600	.15000	---
$(C_{mq})_{wf_R}$	-1.3476	-1.2964	-1.2907	-1.3823	-.78130	-.45240
Parameters pertinent to determination of predicted contributions of canard to variation of C_N and C_m with q and $\dot{\alpha}$						
l_{c_1} , m (ft)	26.28 (86.21)	26.58 (87.22)	26.10 (85.64)	25.63 (84.10)	25.70 (84.33)	25.40 (83.32)
l_{c_2} , m (ft)	21.64 (71.00)	21.64 (71.00)	21.64 (71.00)	21.64 (71.00)	21.64 (71.00)	21.64 (71.00)

TABLE 5. — PREDICTED FLEXIBLE-TO-RIGID RATIOS OF STABILITY AND CONTROL DERIVATIVES FOR FLIGHT-TEST CONDITIONS INVESTIGATED

[From ref. 4]

	Case number											
	SC-1		SC-2		SC-3		SC-4		SC-6		SC-7	
	Lift	Moment	Lift	Moment	Lift	Moment	Lift	Moment	Lift	Moment	Lift	Moment
At $\alpha = 0^\circ$	0.918	0.852	0.882	0.843	0.700	0.672	0.756	0.734	0.903	0.844	0.732	0.742
Angle of attack, wing/fuselage	.990	.941	.987	.943	.975	.906	.983	.926	1.018	1.019	1.007	.990
Angle of attack, canard ¹	-11.980	1.201	-7.538	1.124	-6.218	1.290	-3.114	1.229	-.031	1.284	.809	1.141
Angle of attack, canard interference	1.115	.761	1.101	.805	1.144	.675	1.125	.678	1.169	.711	1.094	.881
Angle of attack, airplane	.954	.717	.963	.760	.935	.700	.951	.780	.983	.803	.995	.885
Canard deflection ¹	-2.154	1.183	-1.020	1.115	-2.820	1.289	-1.579	1.221	-.010	1.255	.827	1.118
Elevon deflection	.738	.774	.844	.861	.601	.659	.707	.749	.689	.736	.834	.835
Geared control deflection	.759	.813	.858	.885	.696	.807	.781	.859	.753	.865	.836	.919
Pitch rate, wing/fuselage	.898	.880	.927	.916	.667	.653	.755	.746	.819	.838	.911	.926
Pitch rate, airplane	.959	.959	.969	.966	.754	.810	.820	.860	.931	.973	.968	.997
$\dot{\alpha}$, wing/fuselage	.946	.952	.986	.988	72.545	.238	57.975	.348	-.925	.357	---	---
$\dot{\alpha}$, airplane	.990	.995	1.015	1.031	1.883	.373	.678	.442	2.135	.500	1.091	.881

¹Includes interference effects.

TABLE 6. — PREDICTED RIGID AND FLEXIBLE AIRPLANE VALUES OF C_{N_α} AND C_{m_α}

$$(a) \left(C_{N_\alpha} \right)_F = \left(\frac{F}{R} \right) \left(C_{N_\alpha} \right)_{wf} + \left(\frac{F}{R} \right) \bar{C}_{N_\alpha c} \left(\bar{C}_{N_\alpha c} \right)_R = \left(\frac{F}{R} \right) C_{N_\alpha} \left(C_{N_\alpha} \right)_R$$

①	②	③	④	⑤	⑥	⑦	⑧
	Table 4		Table 5			-----	-----
Case number	$\left(C_{N_\alpha} \right)_{wf} R$	$\left(\bar{C}_{N_\alpha c} \right)_R$ (1)	$\left(\frac{F}{R} \right) \left(C_{N_\alpha} \right)_{wf}$	$\left(\frac{F}{R} \right) \bar{C}_{N_\alpha c}$	$\left(\frac{F}{R} \right) C_{N_\alpha}$	$\left(C_{N_\alpha} \right)_R =$ $(2) + (3) \frac{1}{57.3}$, per deg	$\left(C_{N_\alpha} \right)_F =$ $(2) (4) + (3) (5) \frac{1}{57.3} =$ $(6) (7)$, per deg
SC-1	2.5302	0.00713	0.990	-11.98	0.954	0.0443	0.0422
SC-2	2.5273	.00711	.987	-7.538	.963	.0442	.0426
SC-3	2.3862	.01321	.975	-6.218	.935	.0419	.0392
SC-4	2.4310	.01862	.983	-3.114	.951	.0428	.0407
SC-6	1.7696	.06064	1.018	-0.031	.983	.0320	.0314
SC-7	1.3995	.08938	1.007	0.809	.995	.0260	.0259

$$(\bar{C}_{N_\alpha c})_R = \left(C_{N_\alpha c} \right)_R + \left(C_{N_\alpha c} \right)_{I_R}$$

$$(b) \left(C_{m_\alpha} \right)_F = \left(\frac{F}{R} \right) \left(C_{m_\alpha} \right)_{wf} + \left(\frac{F}{R} \right) \bar{C}_{m_\alpha c} \left(\bar{C}_{m_\alpha c} \right)_R = \left(\frac{F}{R} \right) C_{m_\alpha} \left(C_{m_\alpha} \right)_R$$

①	②	③	④	⑤	⑥	⑦	⑧
	Table 4		Table 5			-----	-----
Case number	$\left(C_{m_\alpha} \right)_{wf} R$	$\left(\bar{C}_{m_\alpha c} \right)_R$ (1)	$\left(\frac{F}{R} \right) \left(C_{m_\alpha} \right)_{wf}$	$\left(\frac{F}{R} \right) \bar{C}_{m_\alpha c}$	$\left(\frac{F}{R} \right) C_{m_\alpha}$	$\left(C_{m_\alpha} \right)_R =$ $(2) + (3) \frac{1}{57.3}$, per deg	$\left(C_{m_\alpha} \right)_F =$ $(2) (4) + (3) (5) \frac{1}{57.3} =$ $(6) (7)$, per deg
SC-1	-0.42680	0.19727	0.941	1.201	0.717	-0.00400	-0.00287
SC-2	-.39157	.19706	.943	1.124	.760	-.00339	-.00258
SC-3	-.55483	.19476	.906	1.290	.700	-.00628	-.00439
SC-4	-.60661	.19731	.926	1.229	.780	-.00714	-.00557
SC-6	-.34879	.15627	1.019	1.284	.803	-.00336	-.00270
SC-7	-.26654	.10951	.990	1.141	.885	-.00274	-.00242

$$(\bar{C}_{m_\alpha c})_R = \left(C_{m_\alpha c} \right)_R + \left(C_{m_\alpha c} \right)_{I_R}$$

TABLE 7. — PREDICTED RIGID AND FLEXIBLE AIRPLANE VALUES OF $C_{N_{\delta_e}}$ AND $C_{m_{\delta_e}}$

$$(a) \quad \left(C_{N_{\delta_e}} \right)_F = \left(\frac{F}{R} \right) \left(C_{N_{\delta_e}} \right)_{wf} + \left(\frac{F}{R} \right) \bar{C}_{N_{\delta_c}} \left[\frac{\delta_c}{\delta_e} \left(\bar{C}_{N_{\delta_c}} \right)_R \right] = \left(\frac{F}{R} \right) C_{N_{\bar{\delta}_e}} \left(C_{N_{\bar{\delta}_e}} \right)_R$$

①	②	③	④	⑤	⑥	⑦	⑧
Case number	Table 4		Table 5			-----	
	$\left(C_{N_{\delta_e}} \right)_R$	$\left(\bar{C}_{N_{\delta_c}} \right)_R$ (1)	$\left(\frac{F}{R} \right) \left(C_{N_{\delta_e}} \right)_{wf}$	$\left(\frac{F}{R} \right) \bar{C}_{N_{\delta_c}}$	$\left(\frac{F}{R} \right) C_{N_{\bar{\delta}_e}}$	$\left(C_{N_{\bar{\delta}_e}} \right)_R =$ $(2) - 0.15 (3) \frac{1}{57.3}$, per deg	$\left(C_{N_{\bar{\delta}_e}} \right)_F =$ $(2)(4) - 0.15 (3)(5) \frac{1}{57.3} =$ $(6)(7), \text{ per deg}$
SC-1	0.43960	0.02071	0.738	-2.154	0.759	0.00762	0.00578
SC-2	.44044	.02187	.844	-1.020	.858	.00763	.00655
SC-3	.09911	.01707	.601	-2.820	.696	.00168	.00117
SC-4	.09727	.02037	.707	-1.579	.781	.00164	.00128
SC-6	.07371	.04078	.689	-.010	.753	.00118	.00089
SC-7	.04392	.06879	.834	.827	.836	.00059	.00049

$$^1 \left(\bar{C}_{N_{\delta_c}} \right)_R = \left(C_{N_{\delta_c}} \right)_R + \left(C_{N_{\delta_c}} \right)_{I_R} .$$

$$(b) \quad \left(C_{m_{\delta_e}} \right)_F = \left(\frac{F}{R} \right) \left(C_{m_{\delta_e}} \right)_{wf} + \left(\frac{F}{R} \right) \bar{C}_{m_{\delta_c}} \left[\frac{\delta_c}{\delta_e} \left(\bar{C}_{m_{\delta_c}} \right)_R \right] = \left(\frac{F}{R} \right) C_{m_{\bar{\delta}_e}} \left(C_{m_{\bar{\delta}_e}} \right)_R$$

①	②	③	④	⑤	⑥	⑦	⑧
Case number	Table 4		Table 5			-----	
	$\left(C_{m_{\delta_e}} \right)_R$	$\left(\bar{C}_{m_{\delta_c}} \right)_R$ (1)	$\left(\frac{F}{R} \right) \left(C_{m_{\delta_e}} \right)_{wf}$	$\left(\frac{F}{R} \right) \bar{C}_{m_{\delta_c}}$	$\left(\frac{F}{R} \right) C_{m_{\bar{\delta}_e}}$	$\left(C_{m_{\bar{\delta}_e}} \right)_R =$ $(2) - 0.15 (3) \frac{1}{57.3}$, per deg	$\left(C_{m_{\bar{\delta}_e}} \right)_F =$ $(2)(4) - 0.15 (3)(5) \frac{1}{57.3} =$ $(6)(7), \text{ per deg}$
SC-1	-0.22406	0.15552	0.774	1.183	0.813	-0.00432	-0.00351
SC-2	-.21788	.15613	.861	1.115	.885	-.00421	-.00373
SC-3	-.06819	.13947	.659	1.289	.807	-.00156	-.00125
SC-4	-.06897	.14036	.749	1.221	.859	-.00157	-.00135
SC-6	-.05200	.11492	.736	1.255	.865	-.00121	-.00105
SC-7	-.03243	.09182	.835	1.118	.919	-.00081	-.00074

$$^1 \left(\bar{C}_{m_{\delta_c}} \right)_R = \left(C_{m_{\delta_c}} \right)_R + \left(C_{m_{\delta_c}} \right)_{I_R} .$$

TABLE 8. - PREDICTED RIGID AND FLEXIBLE AIRPLANE VALUES OF C_{N_q} , $C_{N_{\dot{\alpha}}}$, $C_{N_q} + C_{N_{\dot{\alpha}}}$

$$(a) \left(C_{N_q} \right)_F = \left(\frac{F}{R} \right)_{C_{N_q}} \left(C_{N_q} \right)_{wf_R} + \left(\frac{F}{R} \right)_{\bar{C}_{N_{\dot{\alpha}}}} \left(\bar{C}_{N_q} \right)_{C_R} = \left(\frac{F}{R} \right)_{C_{N_q}} \left(C_{N_q} \right)_R$$

①	②	③	④	⑤	⑥	⑦	⑧	⑨	⑩	
Case number	Table 4		Table 6(a)	-----			Table 5		-----	
	l_{c_1} m (ft)	$\left(C_{N_q} \right)_{wf_R}$	$\left(\bar{C}_{N_{\dot{\alpha}}} \right)_R$	$\left(\bar{C}_{N_q} \right)_{C_R}$ - 0.0255 ② ④ (1)	$\left(\frac{F}{R} \right)_{C_{N_q}}$ wf	$\left(\frac{F}{R} \right)_{\bar{C}_{N_{\dot{\alpha}}}}$	$\left(\frac{F}{R} \right)_{C_{N_q}}$	$\left(C_{N_q} \right)_R$ ③ + ⑤, per rad	$\left(C_{N_q} \right)_F$ ③ ⑥ + ⑤ ⑦, per rad	
SC-1	26.28 (86.21)	3.3475	0.00713	-0.0156	0.898	-11.980	0.959	3.3319	3.194	
SC-2	26.58 (87.22)	3.1859	.00711	-.0158	.927	-7.538	.969	3.1701	3.072	
SC-3	26.10 (85.64)	2.3049	.01321	-.0289	.667	-6.218	.754	2.2760	1.717	
SC-4	25.63 (84.10)	2.3690	.01862	-.0400	.755	-3.114	.820	2.3290	1.913	
SC-6	25.70 (84.33)	1.1310	.06064	-.1303	.819	-.031	.931	1.0007	.931	
SC-7	25.40 (83.32)	.5359	.08938	-.1894	.911	.809	.968	.3465	.335	

$$^1 \left(C_{N_q} \right)_{C_R} = - \frac{2l_{c_1}}{c_w} \left(C_{N_{\dot{\alpha}}} \right)_R$$

$$(b) \left(C_{N_{\dot{\alpha}}} \right)_F = \left(\frac{F}{R} \right)_{C_{N_{\dot{\alpha}}}} \left(C_{N_{\dot{\alpha}}} \right)_{wf_R} + \left(\frac{F}{R} \right)_{\left(C_{N_{\dot{\alpha}}} \right)_I} \left(C_{N_{\dot{\alpha}}} \right)_{C_{I_R}} = \left(\frac{F}{R} \right)_{C_{N_{\dot{\alpha}}}} \left(C_{N_{\dot{\alpha}}} \right)_R$$

①	②	③	④	⑤	⑥	⑦	⑧	⑨	
Case number	Table 4		-----			Table 5		-----	
	$\left(C_{N_{\dot{\alpha}}} \right)_{wf_R}$	$\left(C_{N_{\dot{\alpha}}} \right)_{I_R}$	$\left(C_{N_{\dot{\alpha}}} \right)_{C_{I_R}} =$ - 1.81 ③ (1)	$\left(\frac{F}{R} \right)_{C_{N_{\dot{\alpha}}}}$ wf	$\left(\frac{F}{R} \right)_{C_{N_{\dot{\alpha}}}}$ $\left(C_{N_{\dot{\alpha}}} \right)_I$	$\left(\frac{F}{R} \right)_{C_{N_{\dot{\alpha}}}}$	$\left(C_{N_{\dot{\alpha}}} \right)_R$ ② + ④, per rad	$\left(C_{N_{\dot{\alpha}}} \right)_F$ ② ⑤ + ④ ⑥, per rad	
SC-1	1.1100	-0.22744	0.4117	0.946	1.115	0.990	1.5217	1.509	
SC-2	1.1200	-.22643	.4098	.986	1.101	1.015	1.5298	1.556	
SC-3	.0042	-.22114	.4003	72.545	1.144	1.883	.4045	.763	
SC-4	.0042	-.22754	.4118	57.975	1.125	.678	.4160	.707	
SC-6	-.0760	-.13404	.2426	-.925	1.169	2.135	.1666	.354	
SC-7	- - -	-.03675	.0665	- - -	1.094	1.091	.0665	.073	

$$^1 \left(C_{N_{\dot{\alpha}}} \right)_{C_{I_R}} = - \frac{2l_{c_2}}{c_w} \left(C_{N_{\dot{\alpha}}} \right)_{I_R} = - 1.81 \left(C_{N_{\dot{\alpha}}} \right)_{I_R} \quad \text{where } l_{c_2} \text{ was obtained from table 4.}$$

$$(c) C_{N_q} + C_{N_{\dot{\alpha}}}$$

①	②d	②b	③d	③b	④a	④b	⑤
Case number	Table 8(a)		Table 8(b)			-----	
	C_{N_q}		$C_{N_{\dot{\alpha}}}$			$C_{N_q} + C_{N_{\dot{\alpha}}}$	$\frac{\left(C_{N_q} + C_{N_{\dot{\alpha}}} \right)_F}{\left(C_{N_q} + C_{N_{\dot{\alpha}}} \right)_R} =$ $\frac{\left(C_{N_q} + C_{N_{\dot{\alpha}}} \right)_R}{\left(C_{N_q} + C_{N_{\dot{\alpha}}} \right)_F} =$ ④b / ④a
	Rigid	Flexible	Rigid	Flexible	Rigid	Flexible	
SC-1	3.3319	3.194	1.5217	1.509	4.8436	4.703	0.969
SC-2	3.1701	3.072	1.5298	1.556	4.6999	4.628	.985
SC-3	2.2760	1.717	.4045	.763	2.6805	2.480	.925
SC-4	2.3290	1.913	.4160	.707	2.7450	2.620	.954
SC-6	1.0007	.931	.1666	.354	1.1673	1.285	1.101
SC-7	.3465	.335	.0665	.073	.4130	.408	.988

TABLE 9. — PREDICTED RIGID AND FLEXIBLE AIRPLANE VALUES OF C_{m_q} , $C_{m_{\dot{\alpha}}}$, $C_{m_q} + C_{m_{\dot{\alpha}}}$

$$(a) \left(C_{m_q} \right)_F = \left(\frac{F}{R} \right) \left(C_{m_q} \right)_{wf_R} + \left(\frac{F}{R} \right) \bar{C}_{m_{\alpha_c}} \left(\bar{C}_{m_q} \right)_{c_R} = \left(\frac{F}{R} \right) C_{m_q} \left(C_{m_q} \right)_R$$

①	②	③	④	⑤	⑥	⑦	⑧	⑨	⑩
Case number	Table 4					Table 5			-----
	l_{c_1} , m (ft)	$\left(C_{m_q} \right)_{wf_R}$	$\left(\bar{C}_{m_{\alpha_c}} \right)_R$	$\left(\bar{C}_{m_q} \right)_{c_R} =$ $-0.0255 \quad (2)(4)$ (1)	$\left(\frac{F}{R} \right) \left(C_{m_q} \right)_{wf}$	$\left(\frac{F}{R} \right) \bar{C}_{m_{\alpha_c}}$	$\left(\frac{F}{R} \right) C_{m_q}$	$\left(C_{m_q} \right)_R =$ $(3) + (5)$, per rad	$\left(C_{m_q} \right)_F =$ $(3)(6) + (5)(7) =$ (8)(9), per rad
SC-1	26.28 (86.21)	-1.3476	0.19727	-0.4337	0.880	1.201	0.959	-1.7813	-1.706
SC-2	26.58 (87.22)	-1.2964	.19706	-.4383	.916	1.124	.966	-1.7347	-1.680
SC-3	26.10 (85.64)	-1.2907	.19476	-.4253	.653	1.290	.810	-1.7160	-1.391
SC-4	25.63 (84.10)	-1.3823	.19731	-.4231	.746	1.229	.860	-1.8054	-1.551
SC-6	25.70 (84.33)	-.7813	.15627	-.3360	.838	1.284	.973	-1.1173	-1.086
SC-7	25.40 (83.32)	-.4524	.10951	-.2327	.926	1.141	.997	-.6851	-.684

$$^1 \left(\bar{C}_{m_q} \right)_{c_R} = - \frac{21}{\bar{c}_w} \left(\bar{C}_{m_{\alpha_c}} \right)_R$$

$$(b) \left(C_{m_{\dot{\alpha}}} \right)_F = \left(\frac{F}{R} \right) \left(C_{m_{\dot{\alpha}}} \right)_{wf_R} + \left(\frac{F}{R} \right) \left(C_{m_{\dot{\alpha}}} \right)_{I_R} = \left(\frac{F}{R} \right) C_{m_{\dot{\alpha}}} \left(C_{m_{\dot{\alpha}}} \right)_R$$

①	②	③	④	⑤	⑥	⑦	⑧	⑨	
Case number	Table 4					Table 5			-----
	$\left(C_{m_{\dot{\alpha}}} \right)_{wf_R}$	$\left(C_{m_{\alpha_c}} \right)_{I_R}$	$\left(C_{m_{\dot{\alpha}}} \right)_{c_R} =$ $-1.81(3)$ (1)	$\left(\frac{F}{R} \right) \left(C_{m_{\dot{\alpha}}} \right)_{wf}$	$\left(\frac{F}{R} \right) \left(C_{m_{\alpha_c}} \right)_I$	$\left(\frac{F}{R} \right) C_{m_{\dot{\alpha}}}$	$\left(C_{m_{\dot{\alpha}}} \right)_R =$ $(2) + (4)$, per rad	$\left(C_{m_{\dot{\alpha}}} \right)_F =$ $(2)(5) + (4)(6) =$ (7)(8), per rad	-----
SC-1	-0.4680	-0.04594	0.0832	0.952	0.761	0.995	-0.3848	-0.3822	
SC-2	-.4470	-.04890	.0885	.988	.805	1.031	-.3585	-.3704	
SC-3	.2360	-.05808	.1051	.238	.675	.373	.3411	.1271	
SC-4	.2360	-.05219	.0945	.348	.678	.442	.3305	.1462	
SC-6	.1500	-.05631	.1019	.357	.711	.500	.2519	.1260	
SC-7	---	-.02654	.0480	---	.881	.881	.0480	.0423	

$$^1 \left(C_{m_{\dot{\alpha}}} \right)_{c_I_R} = - \frac{21}{\bar{c}_w} \left(C_{m_{\alpha_c}} \right)_{I_R} = -1.81 \left(C_{m_{\alpha_c}} \right)_{I_R} \text{ where } l_{c_2} \text{ was obtained from table 4.}$$

$$(c) C_{m_q} + C_{m_{\dot{\alpha}}}$$

①	②a	②b	③a	③b	④a	④b	⑤
Case number	Table 9(a)						-----
	Table 9(b)						-----
	C_{m_q}		$C_{m_{\dot{\alpha}}}$		$C_{m_q} + C_{m_{\dot{\alpha}}}$		$\frac{\left(C_{m_q} + C_{m_{\dot{\alpha}}} \right)_F}{\left(C_{m_q} + C_{m_{\dot{\alpha}}} \right)_R} =$ $\frac{(4b)}{(4a)}$
	Rigid	Flexible	Rigid	Flexible	Rigid	Flexible	
SC-1	-1.7813	-1.706	-0.3848	-0.3822	-2.1661	-2.0882	0.964
SC-2	-1.7347	-1.680	-.3585	-.3704	-2.0932	-2.0504	.980
SC-3	-1.7160	-1.391	.3411	.1271	-1.3749	-1.2639	.919
SC-4	-1.8054	-1.551	.3305	.1462	-1.4749	-1.4048	.952
SC-6	-1.1173	-1.806	.2519	.1260	-.8654	-.9600	1.109
SC-7	-.6851	-.684	.0480	.0423	-.6371	-.6417	1.007

TABLE 10. — FLIGHT-DETERMINED SHORT-PERIOD CHARACTERISTICS
 [Elevator moving during transient oscillations]

	Case number					
	SC-1	SC-2	SC-3	SC-4	SC-6	SC-7
P, sec	5.37	5.63	3.39	3.30	3.88	4.18
ω_{n_d} , rad per sec	1.17	1.113	1.852	1.90	1.62	1.51
ω_n , rad per sec	1.217	1.174	1.915	1.954	1.66	1.53
$T_{1/2}$, sec	2.10	1.85	1.46	1.50	1.80	3.6
ξ	.283	.339	.257	.243	.238	.128
Φ_d , deg	15.8	18.7	14.4	13.6	13.4	7.2
$ \alpha / q $.823	.852	.542	.506	.615	.659
$\Phi_{\alpha q}$, deg	-73.8	-76.3	-86.2	-87.1	-83.4	-86.2
$ a_n / \alpha $, g per rad	16.67	15.6	21.6	20.5	26.5	18.8
$\Phi_{a_n \alpha}$, deg	-.4	2.9	-1.3	7.6	2.9	2.4
$ \delta_e / \alpha $, rad per rad	.478	.425	.437	.410	.425	.277
$\Phi_{\delta_e \alpha}$, deg	-73.8	-82.6	-67.8	-71.1	-77.6	-67.8

TABLE 11. — SUMMARY OF PREDICTED AND FLIGHT-DETERMINED STABILITY AND CONTROL DERIVATIVES

(a) Case number SC-1

Derivative	Predictions				Flight data			
	Original		New		Time vector	Analog	Newton-Raphson	
	Rigid airplane	Flexible airplane	Rigid airplane	Flexible airplane			Without a priori	With a priori
$C_{N\alpha}$, per deg	0.0436	0.0396	0.0443	0.0422	0.0473	0.0486	0.0461	0.0462
$C_{Nq} + C_{N\dot{\alpha}}$, per rad	2.021	.876	4.854	4.703	---	.935	-5.254	-2.017
$C_{N\bar{\delta}_e}$, per deg	.01030	.00650	.00762	.00578	---	.00375	-.00033	.00296
$C_{m\alpha}$, per deg	-0.00362	-0.00170	-0.00400	-0.00287	-0.00146	-0.00129	-0.00133	-0.00139
$C_{mq} + C_{m\dot{\alpha}}$, per rad	-1.486	-1.804	-2.166	-2.088	-1.620	-1.620	-1.795	-1.691
$C_{m\bar{\delta}_e}$, per deg	-.00559	-.00389	-.00432	-.00351	-.00355	-.00372	-.00390	-.00383

(b) Case number SC-2

Derivative	Predictions				Flight data			
	Original		New		Time vector	Analog	Newton-Raphson	
	Rigid airplane	Flexible airplane	Rigid airplane	Flexible airplane			Without a priori	With a priori
$C_{N\alpha}$, per deg	0.0441	0.0422	0.0442	0.0426	0.0476	0.0510	0.0474	0.0476
$C_{Nq} + C_{N\dot{\alpha}}$, per rad	2.019	1.092	4.700	4.628	---	1.790	-4.087	-.166
$C_{N\bar{\delta}_e}$, per deg	.01058	.00740	.00763	.00655	---	.00701	.00042	.00530
$C_{m\alpha}$, per deg	-0.00358	-0.00248	-0.00339	-0.00258	-0.00218	-0.00226	-0.00211	-0.00212
$C_{mq} + C_{m\dot{\alpha}}$, per rad	-1.460	-1.823	-2.093	-2.050	-1.810	-1.900	-1.666	-1.746
$C_{m\bar{\delta}_e}$, per deg	-.00549	-.00458	-.00421	-.00373	-.00380	-.00420	-.00392	-.00410

TABLE 11. — SUMMARY OF PREDICTED AND FLIGHT-DETERMINED STABILITY AND CONTROL DERIVATIVES - Continued

(c) Case number SC-3

Derivative	Predictions				Flight data			
	Original		New		Time vector	Analog	Newton-Raphson	
	Rigid airplane	Flexible airplane	Rigid airplane	Flexible airplane			Without a priori	With a priori
C_{N_α} , per deg	0.0429	0.0380	0.0419	0.0392	0.0434	0.0392	0.0372	0.0396
$C_{N_q} + C_{N_\alpha}$, per rad	2.182	0.870	2.681	2.480	---	.800	-5.230	-3.444
$C_{N_{\bar{\delta}_e}}$, per deg	.00267	.00114	.00168	.00117	---	.00070	-.00019	.00031
C_{m_α} , per deg	-0.00624	-0.00362	-0.00628	-0.00439	-0.00405	-0.00411	-0.00406	-0.00412
$C_{m_q} + C_{m_\alpha}$, per rad	-1.510	-1.684	-1.375	-1.264	-1.410	-1.491	-1.759	-1.642
$C_{m_{\bar{\delta}_e}}$, per deg	-.00221	-.00146	-.00156	-.00125	-.00130	-.00144	-.00150	-.00147

(d) Case number SC-4

Derivative	Predictions				Flight data			
	Original		New		Time vector	Analog	Newton-Raphson	
	Rigid airplane	Flexible airplane	Rigid airplane	Flexible airplane			Without a priori	With a priori
C_{N_α} , per deg	0.0430	0.0401	0.0428	0.0407	0.0479	---	0.0439	0.0451
$C_{N_q} + C_{N_\alpha}$, per rad	2.190	1.080	2.745	2.620	---	---	-7.054	-4.412
$C_{N_{\bar{\delta}_e}}$, per deg	.00269	.00142	.00164	.00128	---	---	-.00026	.00007
C_{m_α} , per deg	-0.00703	-0.00528	-0.00714	-0.00557	-0.00568	---	-0.00570	-0.00579
$C_{m_q} + C_{m_\alpha}$, per rad	-1.554	-1.805	-1.475	-1.405	-1.750	---	-1.684	-1.663
$C_{m_{\bar{\delta}_e}}$, per deg	-.00229	-.00166	-.00157	-.00135	-.00200	---	-.00167	-.00168

TABLE 11. - SUMMARY OF PREDICTED AND FLIGHT-DETERMINED STABILITY AND CONTROL DERIVATIVES - Concluded

(e) Case number SC-6

Derivative	Predictions				Flight data			
	Original		New		Time vector	Analog	Newton-Raphson	
	Rigid airplane	Flexible airplane	Rigid airplane	Flexible airplane			Without a priori	With a priori
$C_{N\alpha}$, per deg	0.0321	0.0309	0.0320	0.0314	0.0394	- - -	0.0326	0.0344
$C_{Nq} + C_{N\dot{\alpha}}$, per rad	1.114	.525	1.167	1.285	- - -	- - -	-1.966	-2.722
$C_{N\bar{\delta}_e}$, per deg	.00169	.00095	.00118	.00089	- - -	- - -	.00059	.00066
$C_{m\alpha}$, per deg	-0.00333	-0.00210	-0.00336	-0.00270	-0.00241	- - -	-0.00229	-0.00237
$C_{mq} + C_{m\dot{\alpha}}$, per rad	-.895	-1.290	-.865	-.960	-1.070	- - -	-1.409	-1.293
$C_{m\bar{\delta}_e}$, per deg	-.00158	-.00115	-.00121	-.00105	-.00108	- - -	-.00116	-.00118

(f) Case number SC-7

Derivative	Predictions				Flight data			
	Original		New		Time vector	Analog	Newton-Raphson	
	Rigid airplane	Flexible airplane	Rigid airplane	Flexible airplane			Without a priori	With a priori
$C_{N\alpha}$, per deg	0.0262	0.0260	0.0260	0.0259	0.0276	0.0259	0.0237	0.0249
$C_{Nq} + C_{N\dot{\alpha}}$, per rad	.623	.316	.413	.408	- - -	1.020	-52.01	-28.77
$C_{N\bar{\delta}_e}$, per deg	.00084	.00065	.00059	.00049	- - -	.00129	.00048	.00058
$C_{m\alpha}$, per deg	-0.00322	-0.00288	-0.00274	-0.00242	-0.00226	-0.00216	-0.00195	-0.00207
$C_{mq} + C_{m\dot{\alpha}}$, per rad	-.589	-.833	-.637	-.642	-.854	-.882	-.717	-.754
$C_{m\bar{\delta}_e}$, per deg	-.00100	-.00083	-.00081	-.00074	-.00078	-.00084	-.00075	-.00076

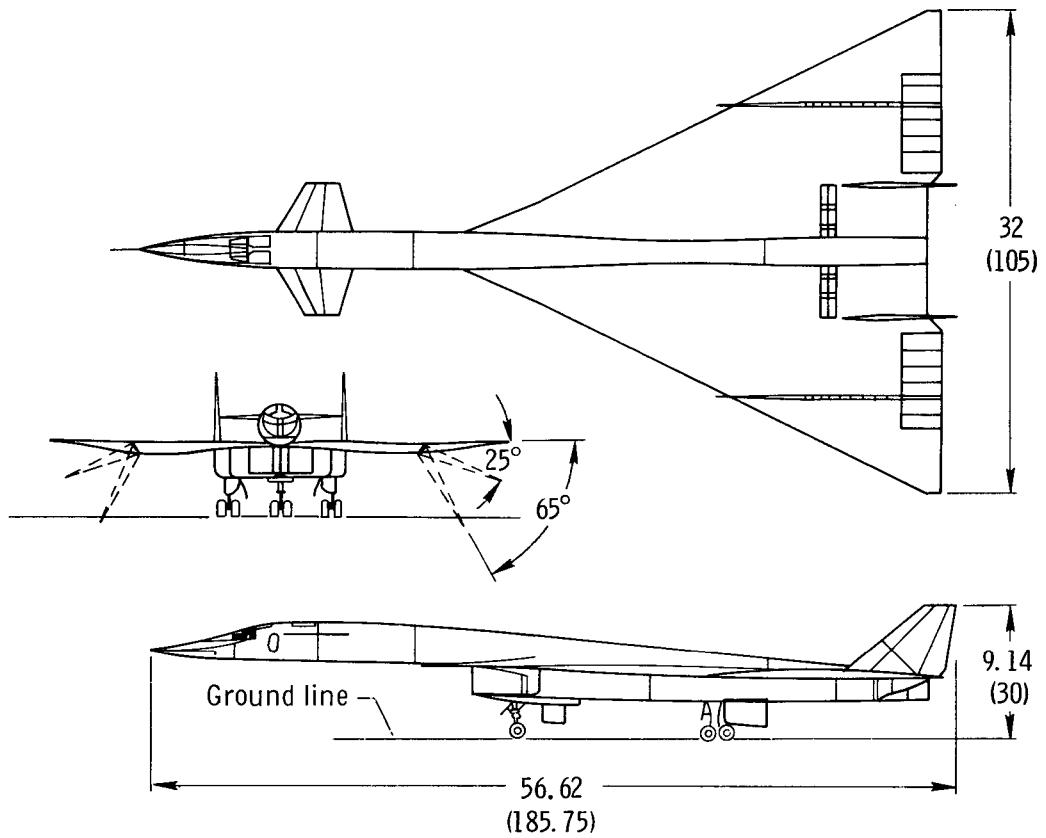


Figure 1. Three-view drawing of XB-70-1 airplane. Dimensions are in meters (feet) except where otherwise noted.

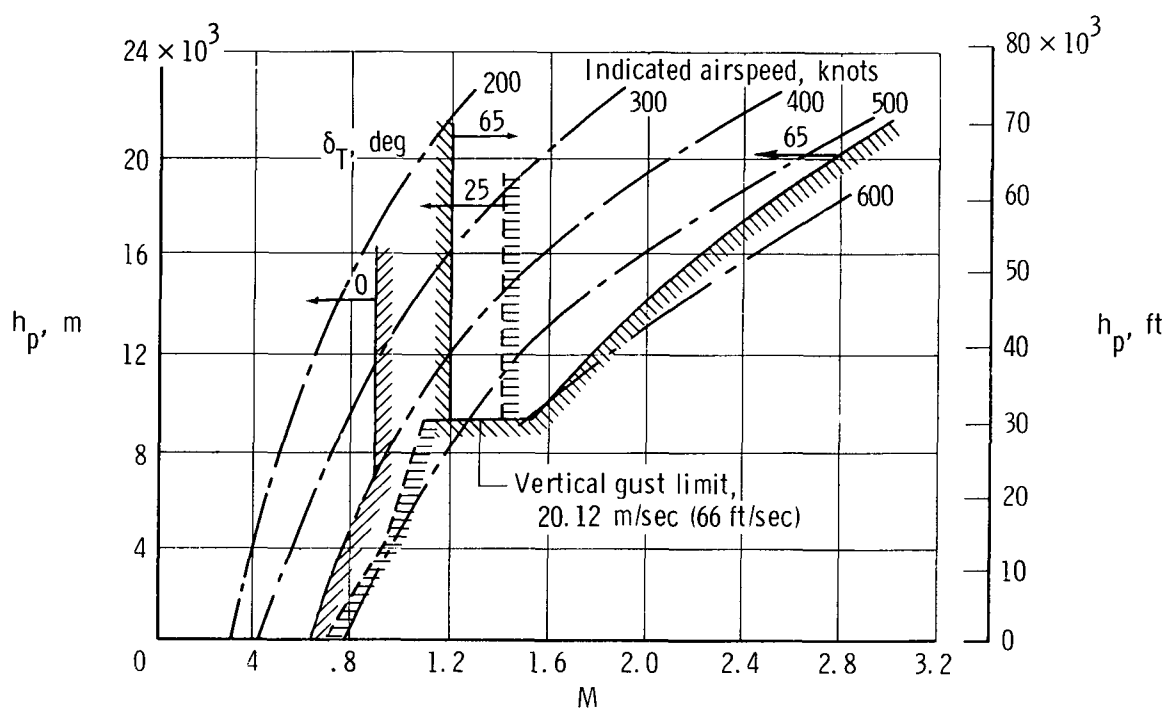


Figure 2. Operational limits of the three wingtip configurations of the XB-70-1.

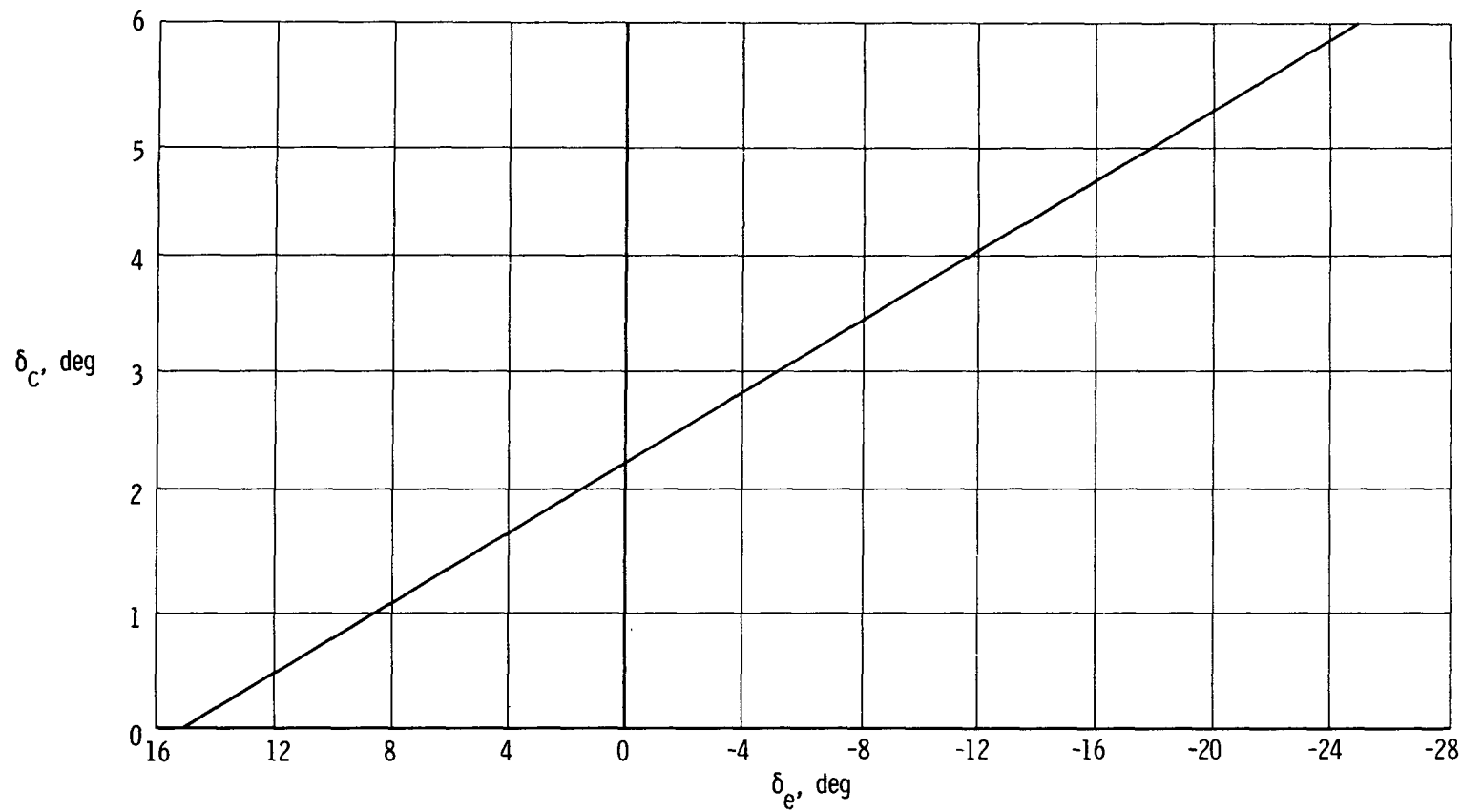
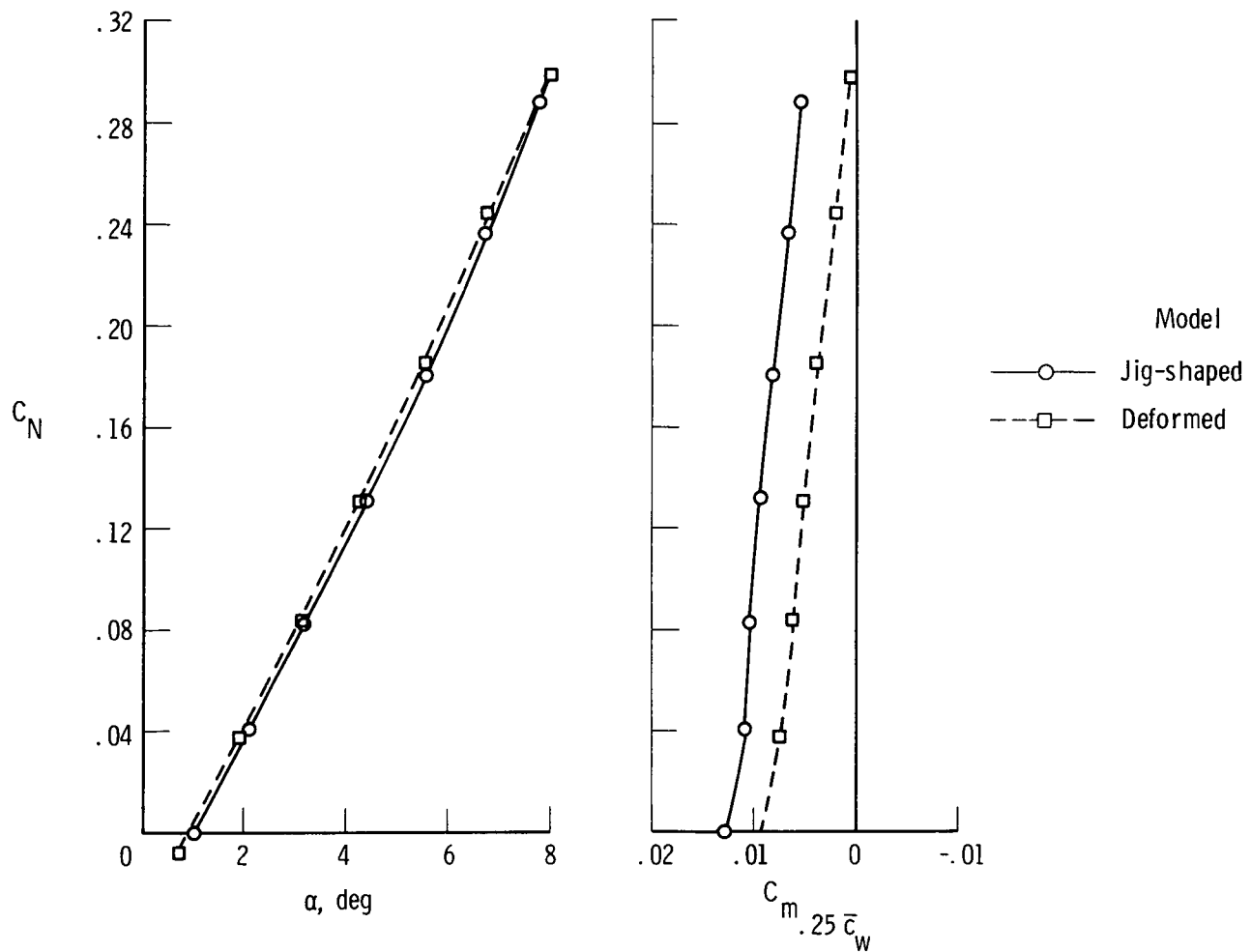
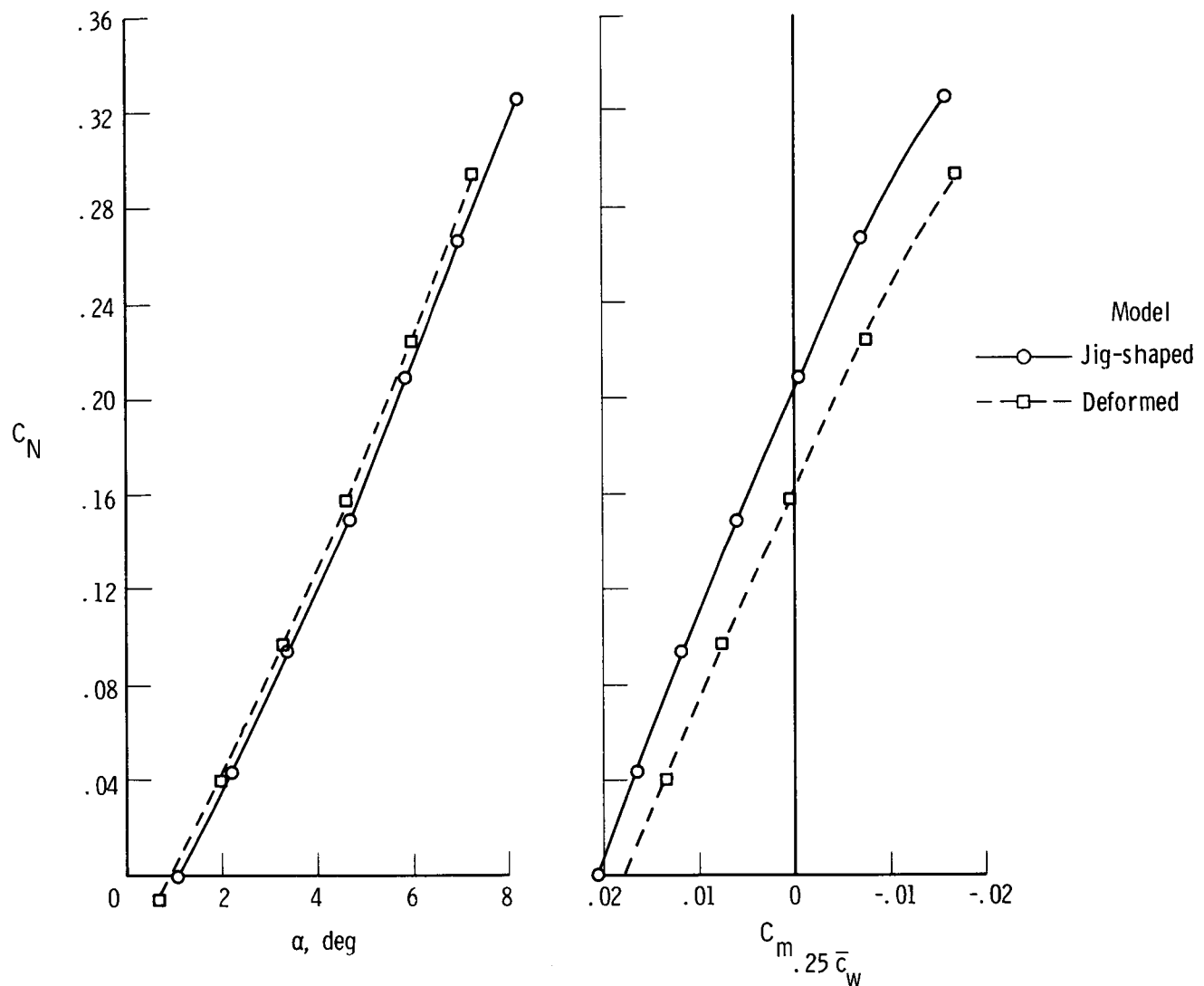


Figure 3. Variation of XB-70-1 canard deflection with elevon deflection. $\delta_c = 2.25^\circ - 0.15\delta_e$.



(a) $M = 0.75$, $\delta_T = 25^\circ$, $N_{Re} = 4 \times 10^6$.

Figure 4. Representative correlations of longitudinal characteristics of XB-70-1 jig-shaped and deformed models based on unpublished 11- by 11-foot Ames wind-tunnel data. $\delta_e = \delta_c = 0^\circ$.



(b) $M = 1.20$, $\delta_T = 25^\circ$, $N_{Re} = 4 \times 10^6$.

Figure 4. Concluded.

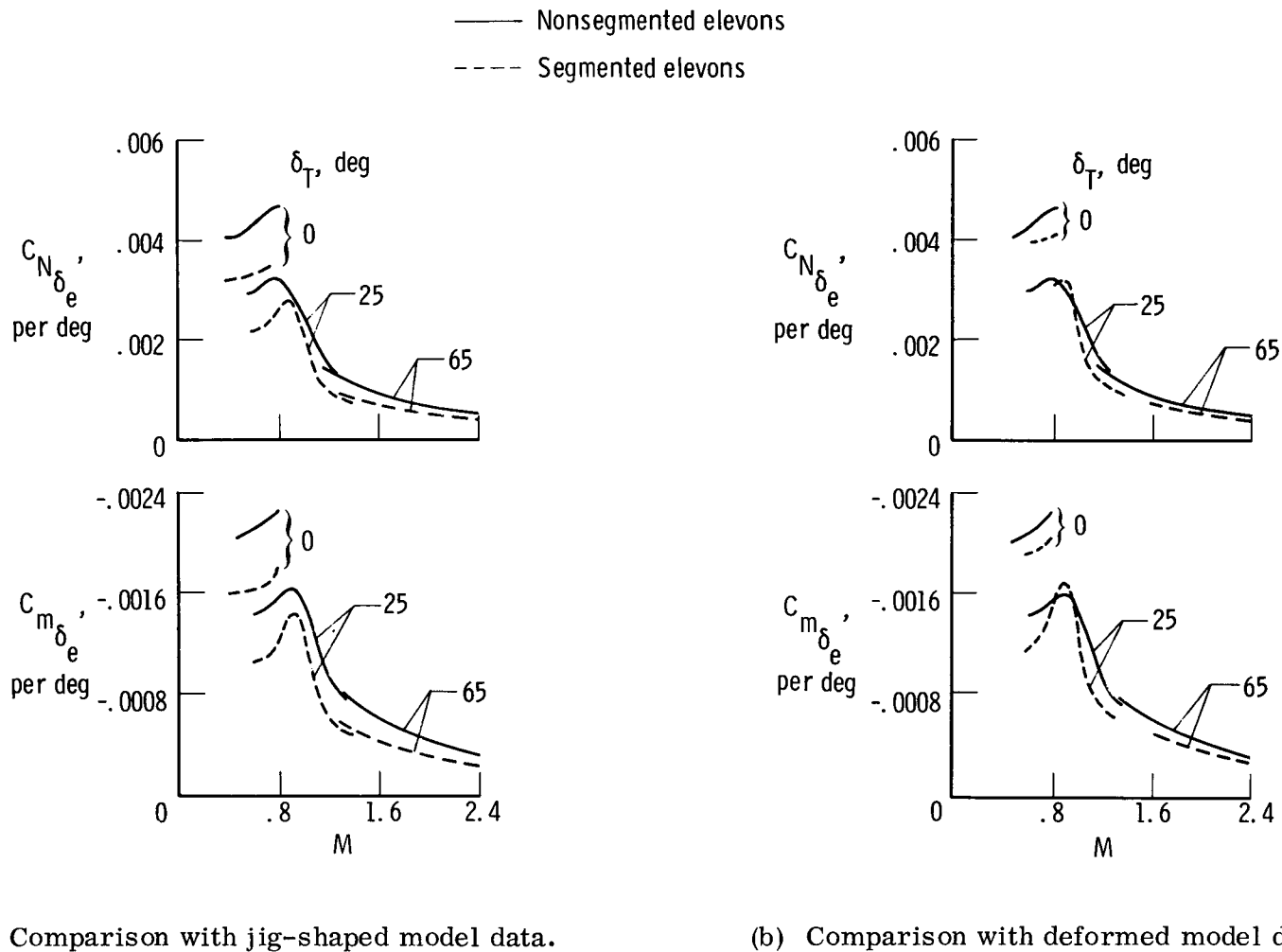


Figure 5. Comparison of elevon effectiveness from original data set (based on nonsegmented elevons) with data for jig-shaped and deformed models (with segmented elevons). $\alpha = 0^\circ$; each plot shows data for elevon segments on one side only.

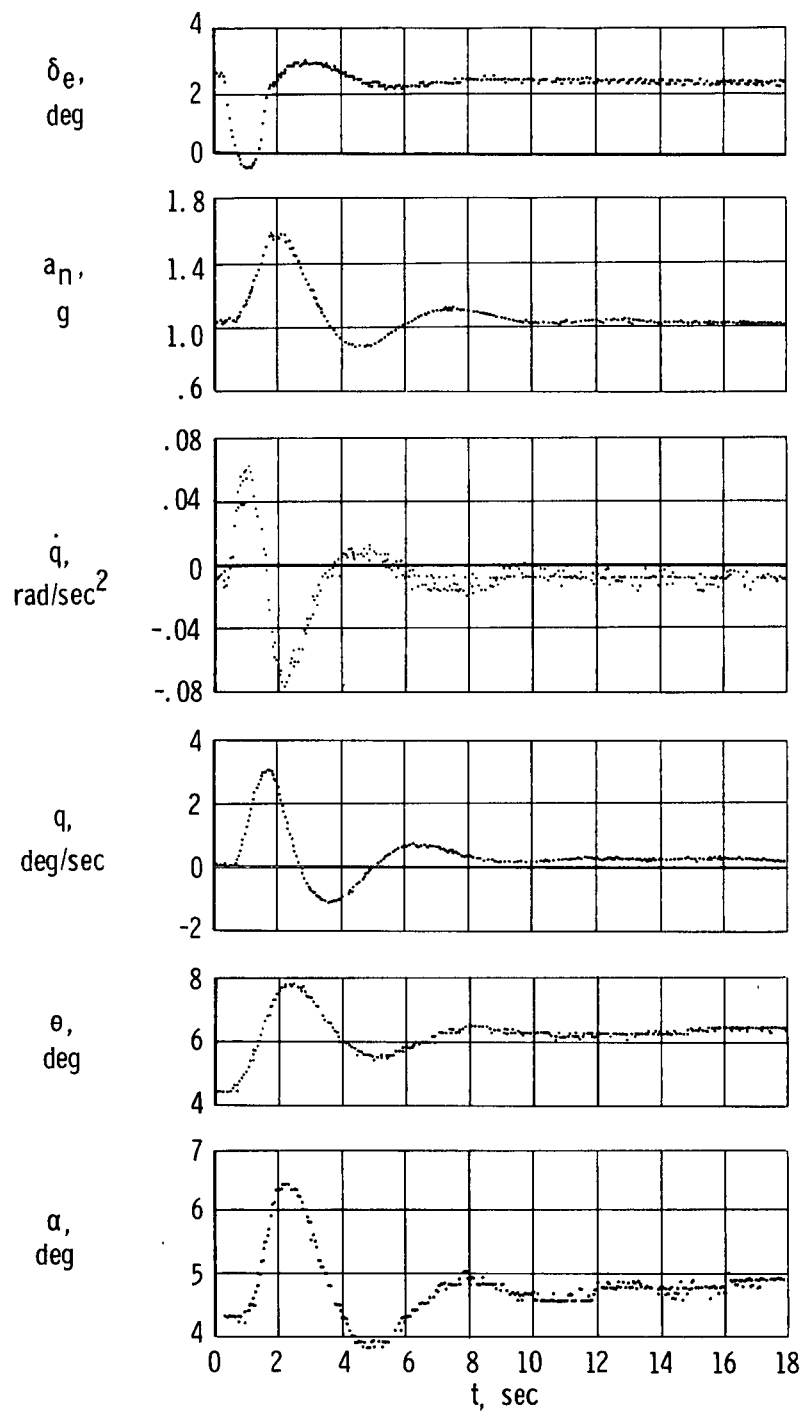
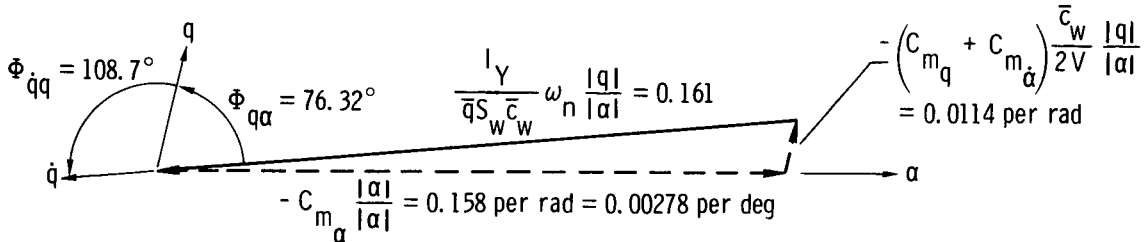


Figure 6. Typical XB-70-1 flight data of pull-up and release maneuver. $M = 0.75$; $\delta_T = 0^\circ$; $W = 1.541 \times 10^5$ kg (3.396×10^5 lb); $h_p = 7650$ m (25,100 ft); center of gravity = $0.234 \bar{c}_w$.

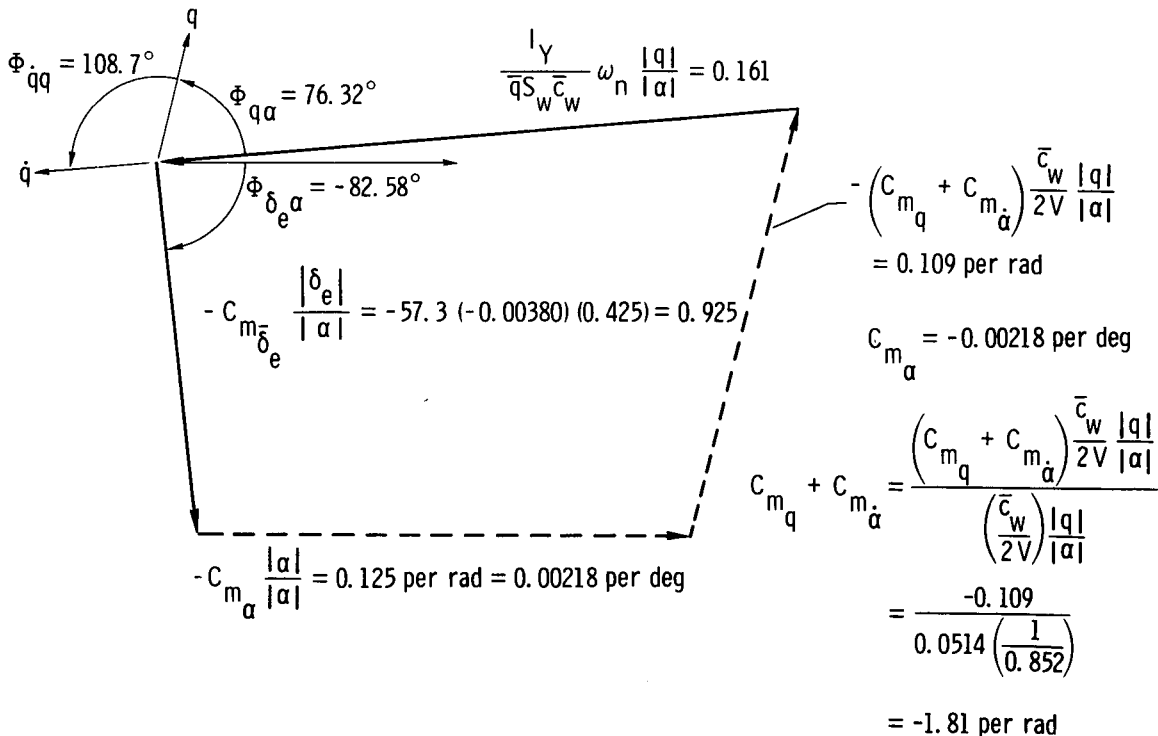
$$\frac{|Y|}{\bar{q}S_w \bar{c}_w} \omega_n \frac{|q|}{|\alpha|} \propto \Phi_{\dot{q}\alpha} - C_{m_\alpha} \frac{|\alpha|}{|\alpha|} \propto \Phi_{\alpha\alpha} - (C_{m_q} + C_{m_{\dot{\alpha}}}) \frac{\bar{c}_w}{2V} \frac{|q|}{|\alpha|} \propto \Phi_{q\alpha} = 0$$



$$C_{m_\alpha} = -0.00278 \text{ per deg}$$

$$C_{m_q} + C_{m_{\dot{\alpha}}} = \frac{(C_{m_q} + C_{m_{\dot{\alpha}}}) \frac{\bar{c}_w}{2V} \frac{|q|}{|\alpha|}}{\left(\frac{\bar{c}_w}{2V}\right) \frac{|q|}{|\alpha|}} = \frac{-0.0114}{0.0514 \left(\frac{1}{0.852}\right)} = -0.189 \text{ per rad}$$

(a) Solution with elevator motion neglected.



(b) Solution with elevator motion accounted for.

Figure 7. Time-vector determination of subsonic longitudinal stability derivatives with oscillatory elevator movements neglected and accounted for. $M = 0.75$; $\delta_T = 0$; $W = 1.541 \times 10^5 \text{ kg}$ ($3.396 \times 10^5 \text{ lb}$); $h_p = 7650 \text{ m}$ (25,100 ft); center of gravity = $0.234 \bar{c}_w$.

$$C_{m_{\bar{\delta}_e}} = \frac{\frac{1}{\gamma} \frac{\bar{c}_w}{q S_w \bar{c}_w} \Delta \dot{q} - C_{m_{\dot{\alpha}}} \Delta \alpha - (C_{m_q} + C_{m_{\dot{q}}}) \frac{\bar{c}_w}{114.6 V} \Delta q}{\Delta \delta_e} = \frac{0.117 \Delta \dot{q} + 0.00218 \Delta \alpha + 0.00162 \Delta q}{\Delta \delta_e}$$

Time, sec	$\Delta \delta_e$, deg	$\Delta \dot{q}$, rad/sec ² (a)	$\Delta \alpha$, deg	Δq , deg/sec (a)	$0.117 \Delta \dot{q}$	$0.00218 \Delta \alpha$	$0.00162 \Delta q$	ΔC_m
0.25	0	0	0	0	0	0	0	0
.30	-.10	.007	0	0	.00082	0	0	.00082
.35	-.30	.012	0	0	.00140	0	0	.00140
.40	-.60	.024	0	0	.00280	0	0	.00280
.45	-1.00	.035	0	.07	.00410	0	.00012	.00422
.50	-1.35	.043	0	.15	.00504	0	.00026	.00530
.55	-1.60	.053	0	.27	.00620	0	.00046	.00666
.60	-2.05	.063	0	.44	.00736	0	.00075	.00811
.65	-2.30	.067	0	.62	.00784	0	.00106	.00890
.70	-2.48	.069	0	.82	.00807	0	.00141	.00948

^aFrom time history adjusted for 0.2-second lag in recorded response.

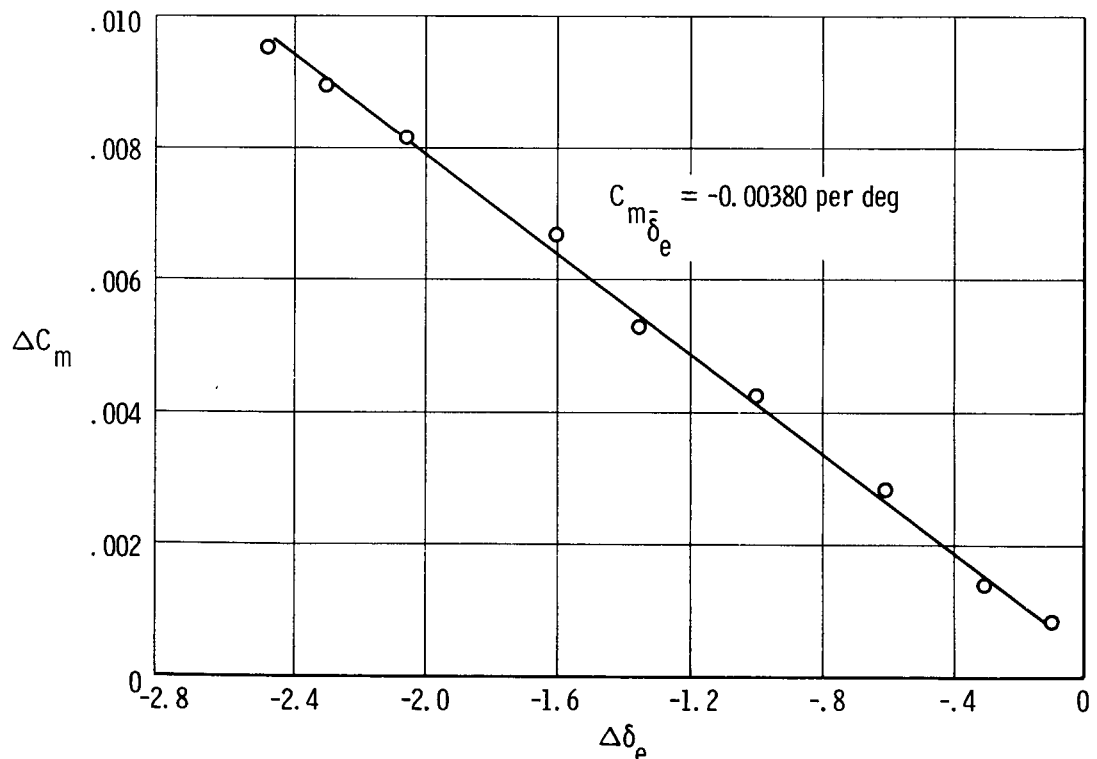
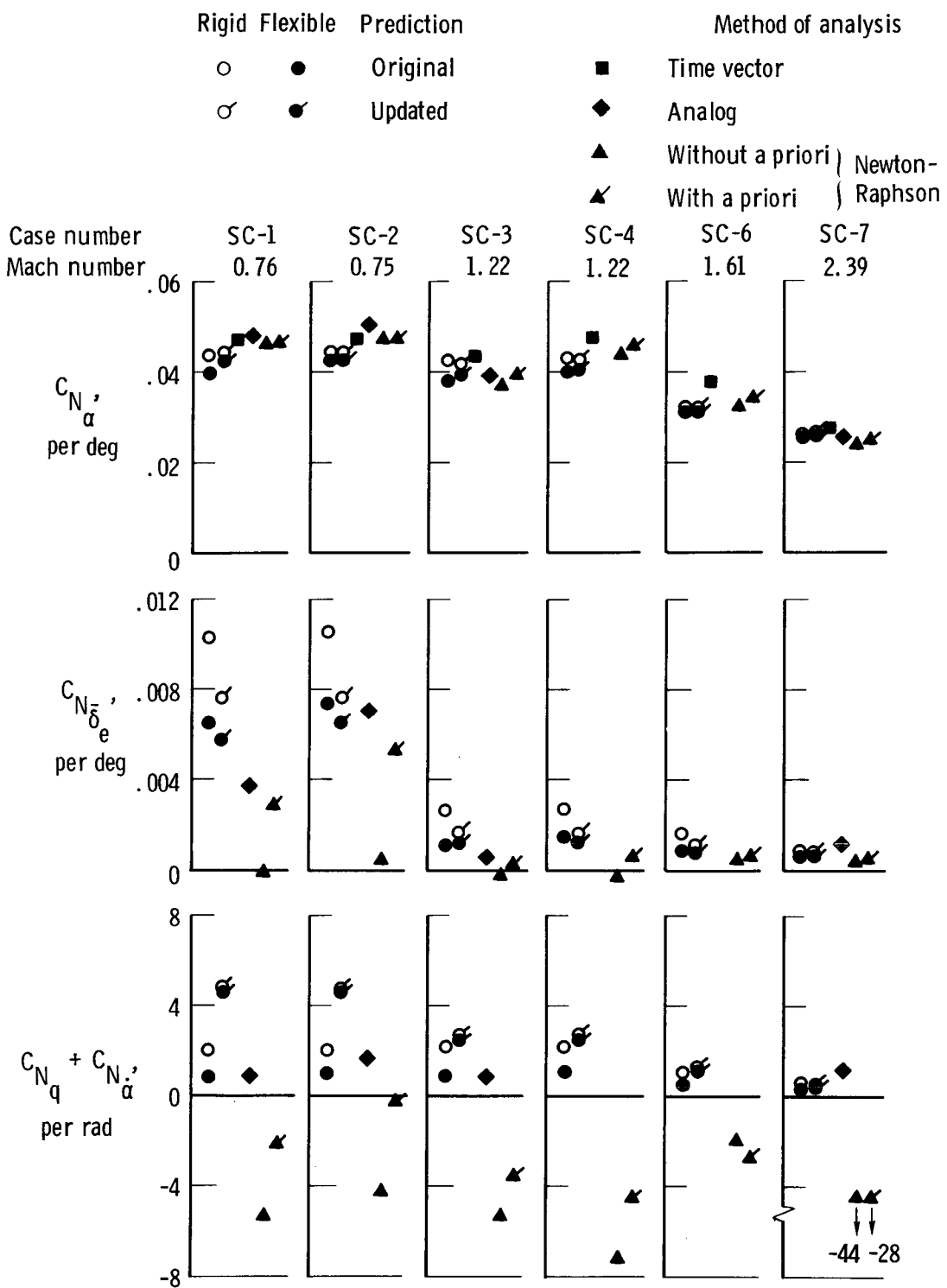
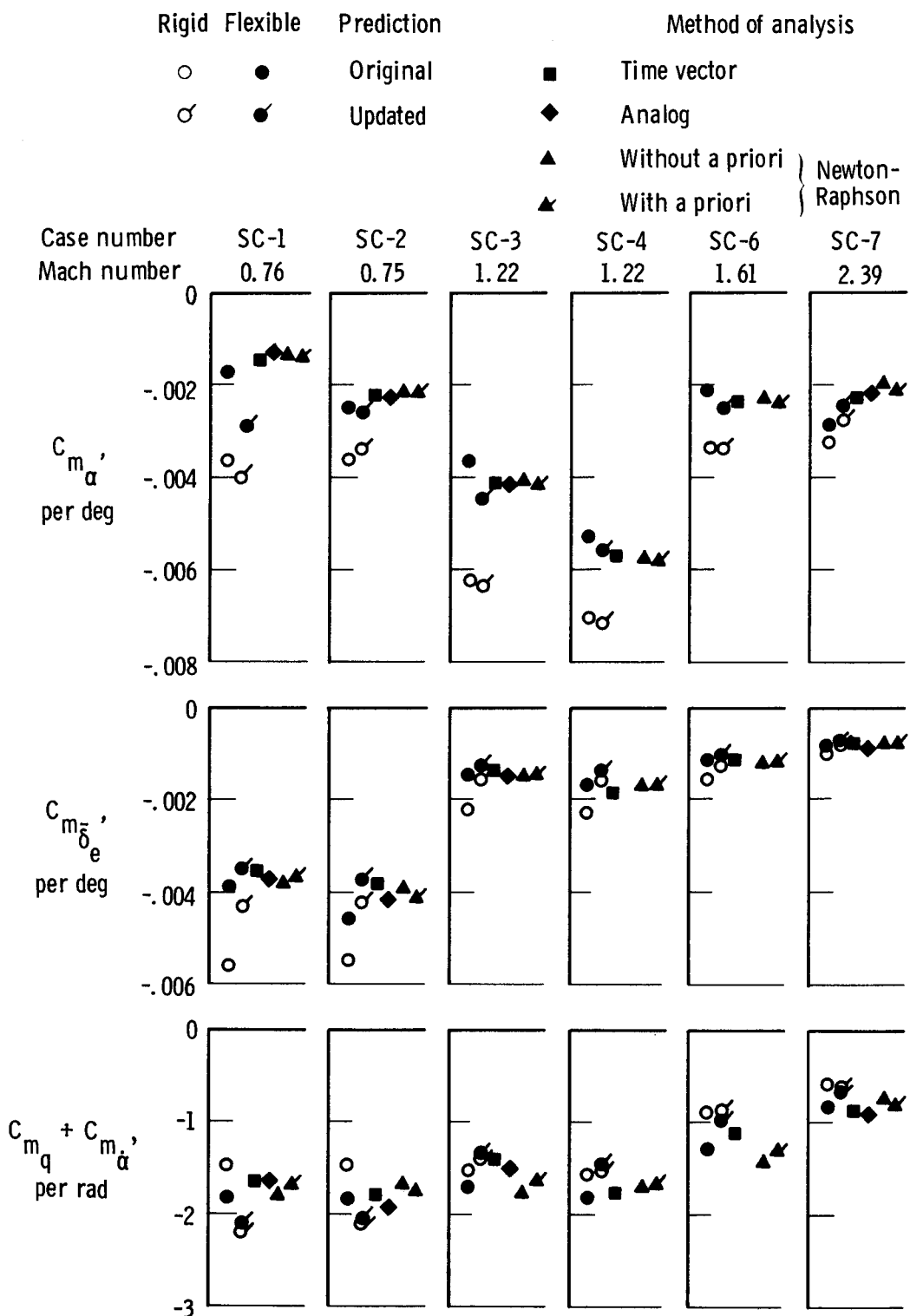


Figure 8. Determination of $C_{m_{\bar{\delta}_e}}$ from desk analysis of initial input and response time histories of figure 6.



(a) Normal-force-coefficient derivatives.

Figure 9. A comparison of flight-determined XB-70-1 longitudinal derivatives with original and updated predictions.



(b) Pitching-moment-coefficient derivatives.

Figure 9. Concluded.

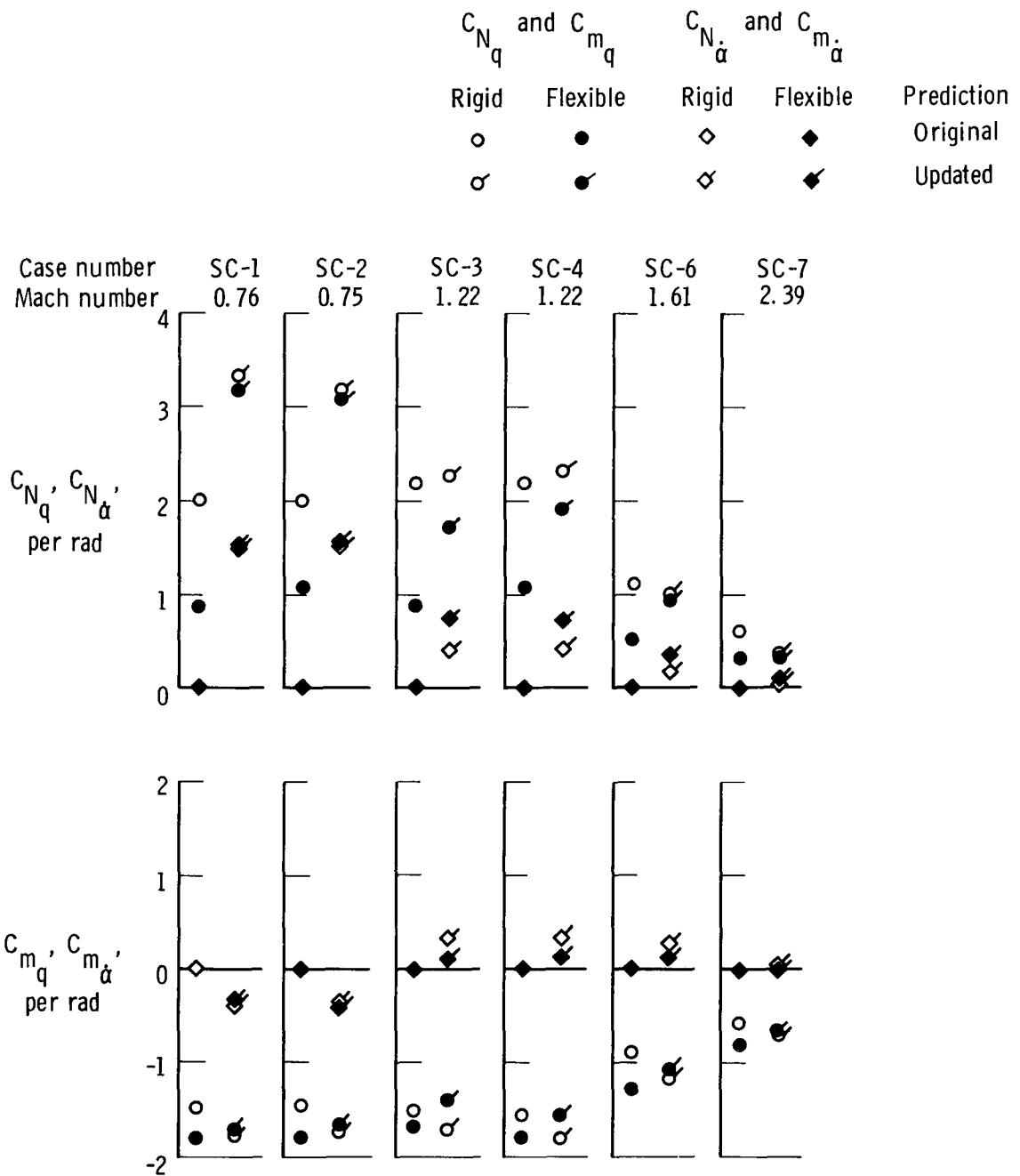


Figure 10. A comparison of updated predicted values of XB-70-1 longitudinal dynamic derivatives relative to q and $\dot{\alpha}$ with original predictions.

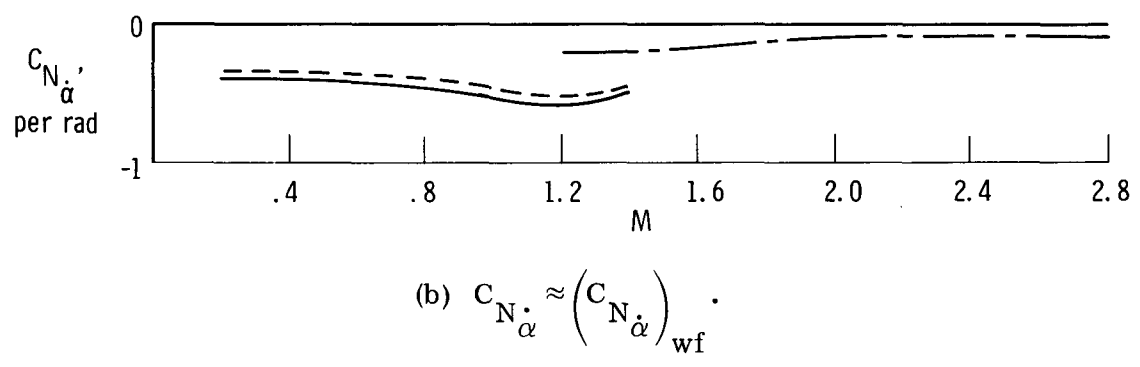
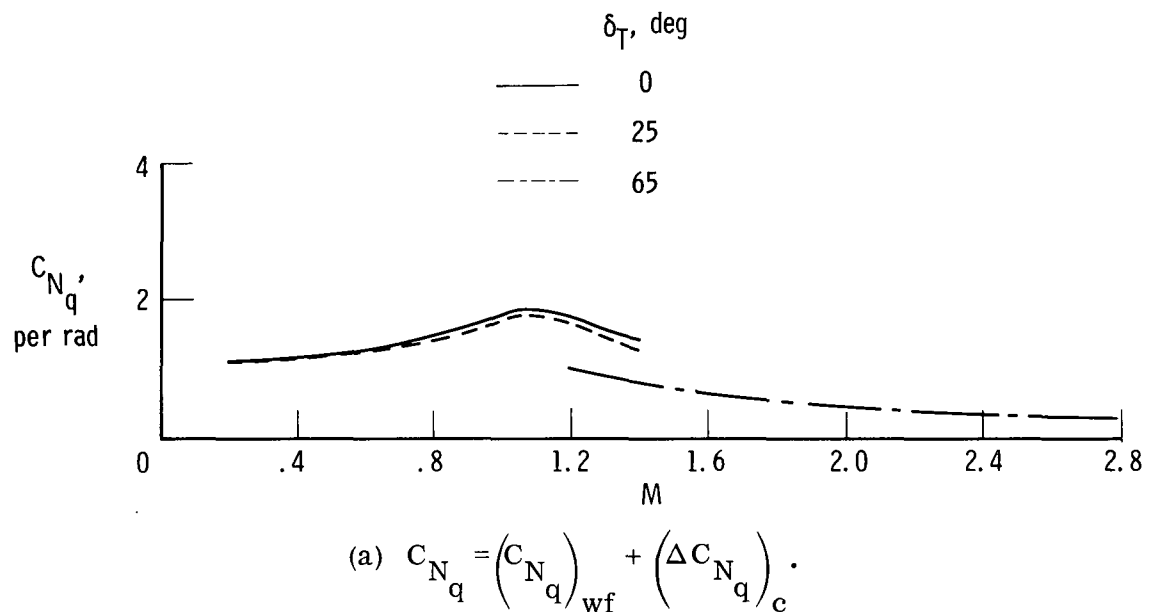


Figure 11. Preliminary estimates of C_{Nq} and $C_{Ndot{\alpha}}$ derived from theoretical and experimental NASA research memorandums, as summarized in reference 4 for the rigid airplane.